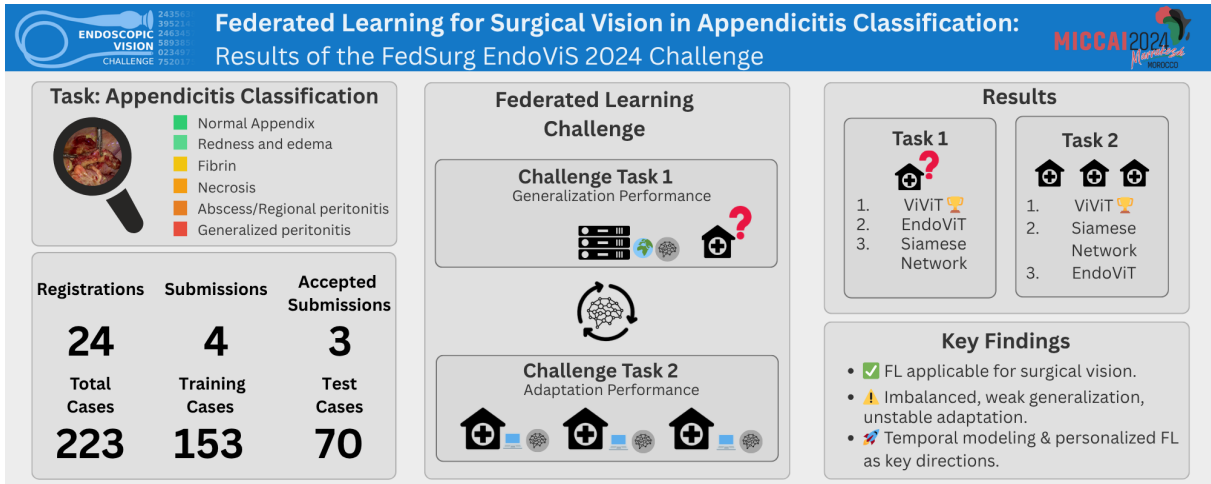


Graphical Abstract

Federated Learning for Surgical Vision in Appendicitis Classification: Results of the FedSurg EndoVis 2024 Challenge

Max Kirchner, Hanna Hoffmann, Alexander C. Jenke, Oliver L. Saldanha, Kevin Pfeiffer, Weam Kanjo, Julia Alekseenko, Claas de Boer, Santhi Raj Kolamuri, Lorenzo Mazza, Nicolas Padoy, Sophia Bano, Annika Reinke, Lena Maier-Hein, Danail Stoyanov, Jakob N. Kather, Fiona R. Kolbinger, Sebastian Bodenstedt, Stefanie Speidel



Highlights

Federated Learning for Surgical Vision in Appendicitis Classification: Results of the FedSurg EndoVis 2024 Challenge

Max Kirchner, Hanna Hoffmann, Alexander C. Jenke, Oliver L. Saldanha, Kevin Pfeiffer, Weam Kanjo, Julia Alekseenko, Claas de Boer, Santhi Raj Kolamuri, Lorenzo Mazza, Nicolas Padoy, Sophia Bano, Annika Reinke, Lena Maier-Hein, Danail Stoyanov, Jakob N. Kather, Fiona R. Kolbinger, Sebastian Bodenstedt, Stefanie Speidel

- First federated learning challenge in surgical AI
- First use of preliminary multi-center Appendix300 dataset
- Novel patient-level video classification beyond image-based tasks
- Findings on generalization vs. personalization in federated learning
- Temporal modeling and personalized FL as key methodological directions

Federated Learning for Surgical Vision in Appendicitis Classification: Results of the FedSurg EndoVis 2024 Challenge

Max Kirchner^{a,*}, Hanna Hoffmann^a, Alexander C. Jenke^a, Oliver L. Saldanha^{d,f}, Kevin Pfeiffer^f, Weam Kanjo^g, Julia Alekseenko^{g,h}, Claas de Boer^a, Santhi Raj Kolamuriⁱ, Lorenzo Mazza^a, Nicolas Padoy^{g,h}, Sophia Bano^l, Annika Reinke^{m,n}, Lena Maier-Hein^{m,n,o,p,q,r}, Danail Stoyanov^{k,l}, Jakob N. Kather^{c,d,f}, Fiona R. Kolbinger^{e,j}, Sebastian Bodenstedt^{a,b}, Stefanie Speidel^{a,b}

^aDepartment of Translational Surgical Oncology, National Center for Tumor Diseases (NCT), NCT/UCC Dresden, a partnership between DKFZ, Faculty of Medicine and University Hospital Carl Gustav Carus, TUD Dresden University of Technology, and Helmholtz-Zentrum Dresden-Rossendorf (HZDR), Dresden, Germany

^bCentre for Tactile Internet with Human-in-the-Loop (CeTI), TUD Dresden University of Technology, Dresden, Germany

^cDepartment of Medicine I, Faculty of Medicine and University Hospital Carl Gustav Carus, TUD Dresden University of Technology, Dresden, Germany

^dMedical Oncology, National Center for Tumor Diseases (NCT), University Hospital Heidelberg, Heidelberg, Germany

^eWeldon School of Biomedical Engineering, Purdue University, West Lafayette, IN, USA

^fElse Kroener Fresenius Center for Digital Health, Faculty of Medicine and University Hospital Carl Gustav Carus, TUD Dresden University of Technology, Dresden, Germany

^gIHU Strasbourg, Institute of Image-Guided Surgery, Strasbourg, France

^hUniversity of Strasbourg, CNRS, INSERM, ICube, UMR7357, Strasbourg, France

ⁱDr. NTR University of Health Sciences, Vijayawada, India

^jDepartment of Visceral, Thoracic and Vascular Surgery, Faculty of Medicine and University Hospital Carl Gustav Carus, TUD Dresden University of Technology, Dresden, Germany

^kDigital Technologies, Medtronic, London, United Kingdom

^lUCL Hawkes Institute and Department of Computer Science, University College London, London, UK

^mGerman Cancer Research Center (DKFZ) Heidelberg, Division of Intelligent Medical Systems, Heidelberg, Germany

ⁿGerman Cancer Research Center (DKFZ) Heidelberg, Helmholtz Imaging, Heidelberg, Germany

^oNational Center for Tumor Diseases (NCT) Heidelberg, a partnership between DKFZ and Heidelberg University Hospital, Heidelberg, Germany

^pFaculty of Mathematics and Computer Science, Heidelberg University, Heidelberg, Germany

^qHelmholtz Information and Data Science School for Health, Heidelberg, Karlsruhe, Germany

^rHeidelberg University Hospital, Surgical Clinic, Surgical AI Research Group, Heidelberg, Germany

^sKrankenhaus St. Joseph-Stift Dresden GmbH, Dresden, Germany

Abstract

Developing generalizable surgical AI requires multi-institutional data, yet patient privacy constraints preclude direct data sharing, making Federated Learning (FL) a natural candidate solution. The application of FL to complex, spatiotemporal surgical video data remains largely unbenchmarked. We present the FedSurg Challenge, the first international benchmarking initiative dedicated to FL in surgical vision, evaluated as a proof-of-concept on a multi-center laparoscopic appendectomy dataset (preliminary subset of Appendix300). Three submissions were evaluated on generalization to an unseen

*Corresponding author

Email address: max.kirchner@nct-dresden.de (Max Kirchner)

center and center-specific adaptation. Centralized and Swarm Learning baselines isolate the contributions of task difficulty and decentralization to observed performance. Even with all data pooled centrally, the task achieved only 26.31% F1-score on the unseen center, while decentralized training introduced an additional, separable performance penalty. Temporal modeling emerges as the dominant architectural factor: video-level spatiotemporal models consistently outperformed frame-level approaches regardless of aggregation strategy. Naive local fine-tuning leads to classifier collapse on imbalanced local data; structured personalized FL with parameter-efficient fine-tuning represents a more principled path toward center-specific adaptation. By characterizing current FL limitations through rigorous statistical analysis, this work establishes a methodological reference point for robust, privacy-preserving AI systems in surgical video analysis.

Keywords: Federated Learning, EndoViS Challenge, Appendectomy, Video Classification, Surgical Data Science

1. Introduction

The combination of early successes in AI algorithms and the emerging field of Surgical Data Science (SDS) holds strong potential to transform surgery [1]. Recent work has demonstrated that AI can reliably analyze surgical video, comprehending anatomy, tool usage, and procedural events in real time [2]. Such capabilities are clinically relevant given the established relationship between video-derived quality indicators and postoperative complications. However, the development of robust AI systems critically depends on access to large volumes of high-quality, diverse surgical data. This requirement remains one of the field’s most pressing challenges [3].

Surgical datasets are typically sourced from either a single institution or a small group of collaborators [3, 4]. While these datasets enable preliminary developments, they inherently suffer from limited diversity and scale if applied in real-world scenarios [5]. Single-center datasets often lack the heterogeneity required for generalizable AI models and involve prolonged data acquisition cycles [6]. Multi-institutional data aggregation, on the other hand, can significantly enrich the dataset, but is frequently obstructed by stringent regulatory frameworks such as the Health Insurance Portability and Accountability Act (HIPAA) [7] or the General Data Protection Regulation (GDPR) [8] that prohibit unrestricted data sharing.

A viable solution is Federated Learning (FL). FL enables decentralized model training across multiple clients, such as hospitals, without the need to share raw image or video data [9]. Instead, the model is brought to the data, preserving privacy and complying with regulations like GDPR or HIPAA. In a standard FL workflow, each client trains a model locally on its private dataset. Only model updates are sent to a central server, where they are aggregated using strategies like Federated Averaging (FedAvg) [9] or more robust alternatives such as FedMedian [10]. The updated global model is then redistributed to clients, and this cycle repeats until convergence.

FL is especially well-suited for medical applications, where data privacy, security, and the lack of standardized datasets pose significant challenges [11]. It enables large-scale collaborative model development without the need to centralize sensitive, multi-institutional data, thereby preserving patient confidentiality and regulatory compliance [11]. However, FL also introduces new challenges. These include handling data and system heterogeneity across institutions [12, 13, 14], balancing personalization with generalization [15], managing communication overhead due to frequent model updates [9, 13], addressing fairness and

potential model biases [13, 16], and coping with the increased complexity of evaluation and debugging in distributed settings [13]. In the context of SDS, recent studies have begun to explore FL for tasks such as surgical phase recognition, scene segmentation, and tool detection [17, 18, 19].

To address challenges in SDS, initiatives such as the Endoscopic Vision (EndoVis) Challenge [20] have become critical accelerators for progress. The Federated Learning for Surgical Vision (FedSurg) challenge, introduced as part of the 2024 edition of EndoVis, represents the first FL challenge in the field of SDS. It aimed to benchmark the state of the art in applying FL to surgical AI for privacy-preserving model development across institutions. In particular, the challenge focused on evaluating model performance in terms of generalization to unseen centers versus adaptation to individual centers, reflecting two core challenges of FL in real-world surgical applications. The Appendix300 dataset is a multi-institutional appendectomy video dataset [21]. As the first FL challenge of its kind in SDS, FedSurg pioneers the use of a preliminary version of the Appendix300 dataset as a foundational platform for algorithm development and validation. A separate study using the complete dataset is published [22]. In this paper, we report the challenge design, results, and findings of FedSurg according to the transparent reporting of biomedical image analysis challenges (BIAS) guidelines [23].

The main contributions of this paper are:

- The design and results of FedSurg, the first international challenge in Surgical Data Science dedicated to Federated Learning, which pioneers the use of the preliminary, multi-center Appendix300 dataset.
- A benchmark of FL strategies for the novel task of patient-level surgical video appendicitis grading classification, advancing the complexity of analysis beyond common static, image-based tasks.
- A rigorous, data-driven analysis of the critical trade-off between model generalization to unseen institutions and personalization to local client data.
- A clear demonstration of the current strengths and practical limitations of FL in surgical AI, highlighted by bootstrapping and Wilcoxon signed-rank test.

2. Challenge Design

This section outlines the design of the FedSurg challenge, detailing its organizational structure, the core mission guiding the competition, and the datasets employed for evaluation. Additionally, it describes the assessment methods used to fairly and rigorously evaluate submitted models and FL settings, ensuring robust comparison across the multi-centric surgical video dataset.

2.1. Challenge Organization

The FedSurg challenge was a one-time event with a fixed submission deadline, held as part of the Medical Image Computing and Computer Assisted Intervention (MICCAI) 2024 conference in Marrakech, Morocco (October 6–10, 2024). Organized jointly by research groups from the Dresden University of Technology (TUD), Purdue University, and the National Center for Tumor Diseases (NCT) Dresden (see Appendix C), the challenge offered a prize pool of €500, provided by the Horizon Europe NearData project and distributed equally between the two challenge tasks.

The primary mission of the FedSurg challenge was to benchmark FL approaches for surgical video classification using a new multi-institutional dataset. The dataset was collected from four German hospitals under institutional ethical approval (see Appendix F). Only training data was released to participants, while test data remained private and was accessible only to the organizers. The dataset used in the FedSurg challenge is a preliminary subset of the Appendix300 dataset [21] (see Subsection 2.3).

All relevant information, including registration, data access, submission progress tracking, guidelines, and a discussion forum, was made available through the official challenge website on Synapse (see Appendix D). This platform served as the central hub for participant onboarding, communication, and submission management. Participants were required to sign challenge rules before they could participate and get access to the data (see Appendix B). The challenge timeline included registration in April 2024, a feedback-based testing phase during August–September, and the final submission deadline on September 18, 2024 (Figure 1).

Participants were restricted to the released training data and publicly available resources, including pre-trained models. Challenge-provided data could not be used for pre-training in FL submissions. Members of the organizing institutes were permitted to participate but were not eligible for awards. More information about the challenge is available in the challenge design document (see Appendix E).

Submissions were required in a containerized format (Docker) and were evaluated on a dedicated server equipped with up to 8 NVIDIA V100 GPUs, 56 CPUs, and 756 GB RAM. This standardized hardware environment and containerized execution ensured reproducibility and fair benchmarking under identical conditions (Figure 1). To support participants, example FL code and evaluation scripts were made publicly available (see Appendix D).

Results were first announced during the MICCAI 2024 Satellite Events and subsequently published on the challenge website, alongside the evaluation framework, rankings, and key performance metrics. All results and analyses from teams with a complete working submission are included in this joint publication, with contributing team members listed as co-authors. Authors were not permitted to publish individual challenge results prior to the release of this paper, ensuring coordinated dissemination and preserving the novelty of the outcomes.

2.2. Challenge Mission

The FedSurg challenge focuses on classifying the inflammatory stage of acute appendicitis using laparoscopic appendectomy videos, an important and commonly performed surgical procedure. The primary objective is to provide a comparative benchmark of existing solutions, with a special emphasis on exploring various FL strategies. In particular, the challenge investigates the balance between personalization and generalization under inherent data heterogeneity. For this purpose, the newly created Appendix300 dataset was introduced, with the challenge of utilizing a partial subset of its data. This makes FedSurg not only the first FL challenge in SDS but also the first benchmarking study of different FL approaches on the patient-level task of appendicitis classification.

The challenge cohort comprises human patients, both adults and children of diverse ages and biological sex, who underwent appendectomy for suspected appendicitis at four German medical centers. In general, the challenge cohort is a representative sample of patients undergoing appendectomy for suspected appendicitis. The dataset consists of laparoscopic video recordings captured during these interventions. While no additional patient data was provided for the challenge, the final Appendix300 dataset includes supplementary clinical information [21].

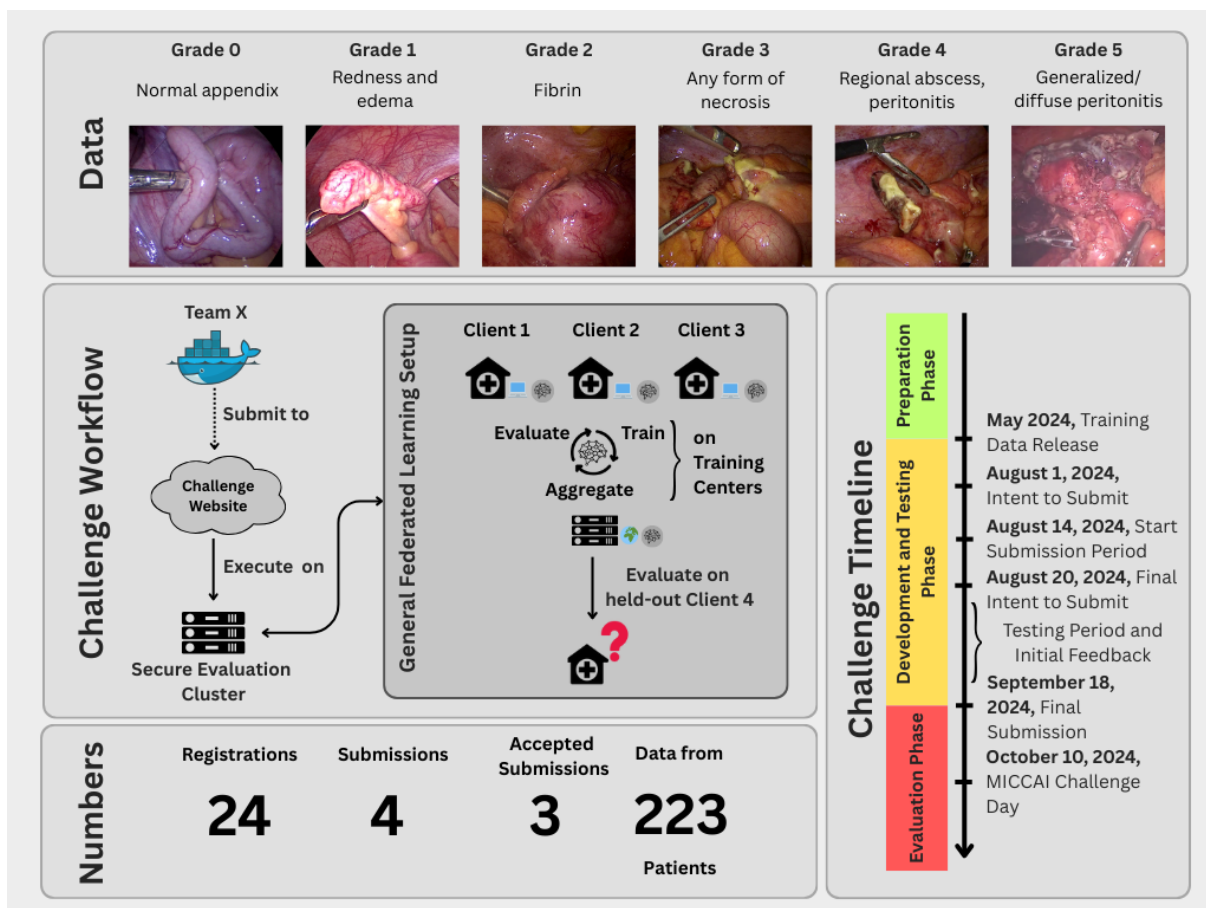


Figure 1: **FedSurg24 Challenge Highlights:** The top panel shows example images of intraoperative appendicitis grades, defined according to Gomes et al. [24], which were used for video annotation. The lower panel illustrates the FedSurg Challenge workflow: teams submitted Docker containers via Synapse, which were executed on a secure cluster simulating FL across three centers with local training and centralized aggregation. Final performance was assessed by testing each center’s best local model on its own test set, while the global model was evaluated on the unseen hold-out center to measure generalization. The challenge timeline with key dates is shown alongside.

This challenge’s main contribution is its patient-level prediction task for appendicitis staging, a transferable innovation for AI in surgery. This challenge serves as a proof-of-concept for applying FL to patient-level surgical video analysis, with methodological insights intended to transfer to future tasks with broader clinical relevance, such as intraoperative decision support or quality control across diverse surgical procedures.

Participants were tasked with developing FL algorithms to classify appendicitis stages in laparoscopic videos, structured around two core tasks:

- Task 1, Generalization: Evaluate the model’s ability to generalize to unseen centers. Participants train their models on a subset of centers and are evaluated on a held-out center that was not involved in training.
- Task 2, Adaptation: Assess the model’s ability to personalize to each center’s test data. Here, the same trained model is fine-tuned (or adapted) for each single center of the federated setup and then evaluated independently on each center’s test set.

In the context of federated learning, generalization is the ability of a collaborative global model to perform well on data from new clients, while personalization involves adapting the model to achieve optimal performance for a specific client’s unique data. The challenge promotes the creation of privacy-preserving algorithms that can tackle both of these issues, creating models that are both robust and adaptable to diverse surgical settings.

2.3. Challenge Dataset

The challenge dataset is a preliminary subset of the Appendix300 collection and comprises frames from 223 full-length recordings of laparoscopic appendectomies. Beyond image frames and laparoscopic grading, the finalized Appendix300 dataset is enriched with detailed histopathological findings and patient anamnesis data [21]. For this challenge, 200 frames were extracted per video using FFmpeg software [25], capturing a 100-second window sampled at two frames per second around an annotated timestamp [21].

Frames were selected at the timestamp identified by the operating surgeon when the appendix was fully visible prior to dissection [21]. Inflammation severity, graded from level 0 to 5, was annotated by the operating surgeon (surgery residents with varying years of experience). The annotation protocol (available at [21]) defines class descriptions and includes illustrative examples based on the definition by Gomes et al. [24]. Furthermore, fine-grained classes 3A/3B were merged into class 3, and classes 4A/4B into class 4 in this challenge dataset. An example overview of the data is visible in Figure 1. By using this annotation protocol, a verbal explanation to the participating surgeons, and a custom graphical user interface of the annotation software, we minimize misclassification. Therefore, we deem the risk of misclassification limited to borderline cases (i.e., cases between partial and total necrosis of the appendix). This potential source of error applies equally to all centers.

The challenge dataset comprises data collected from multiple hospitals across Germany, including both university and community hospitals with varied surgical profiles. While the challenge simulates an FL setup, it reflects a realistic scenario since the data originates from four distinct, real-world centers that have been anonymized to protect institutional privacy. The contributing institutions include:

- Asklepios-ASB Klinik Radeberg

- University Hospital Carl Gustav Carus Dresden, Department of Pediatric Surgery
- Krankenhaus St. Joseph-Stift, Dresden
- St. Elisabethen-Krankenhaus, Ravensburg

An overview of the video distribution across centers is shown in Table 1.

Table 1: Data Distribution Across Participating Centers. Every video is standardized to a 100-second clip, centered on the timestamp of full appendiceal visibility prior to surgical preparation.

| Center | Training Videos | Testing Videos | Total |
|--------|-----------------|----------------|-------|
| 1 | 40 | 10 | 50 |
| 2 | 33 | 9 | 42 |
| 3 | 80 | 22 | 102 |
| 4 | 0 | 29 | 29 |
| Total | 153 | 70 | 223 |

To discourage centralized model development and preserve the integrity of the federated setting, the training data was partitioned into public and private subsets. Participants were granted access only to the public subset, which constituted 25% of the total training data. The remaining 75% was used exclusively by the organizers during the final training phase, where both public and private data were jointly leveraged in a secure federated setup (Figure 1 and Figure 2). The class distribution within the dataset mirrors real-world clinical prevalence, featuring a predominance of mid-level cases and a lower representation of extreme or mild inflammation levels.

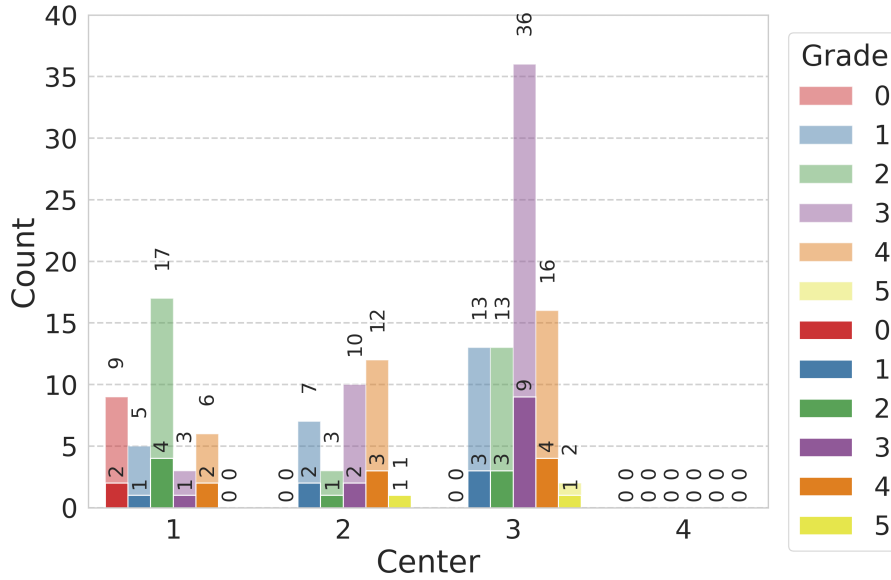
No predefined validation set was provided. Participants were expected to devise their own validation strategies. Final submissions were executed centrally by the organizers, who conducted full federated training and evaluation across all centers under secure and standardized conditions to ensure reproducibility and fairness.

Since the challenge dataset constitutes a preliminary subset of the Appendix300 dataset, we provide a CSV file specifying which samples were used in the challenge here¹. In addition, two videos are released that were excluded from the final dataset because they were either shorter than 100 seconds or did not contain a clearly visible appendix in the center. The Appendix300 dataset is publicly available for non-commercial use under the Creative Commons Attribution (CC BY) license. Any use of this dataset requires citing both this paper and the final Appendix300 publication.

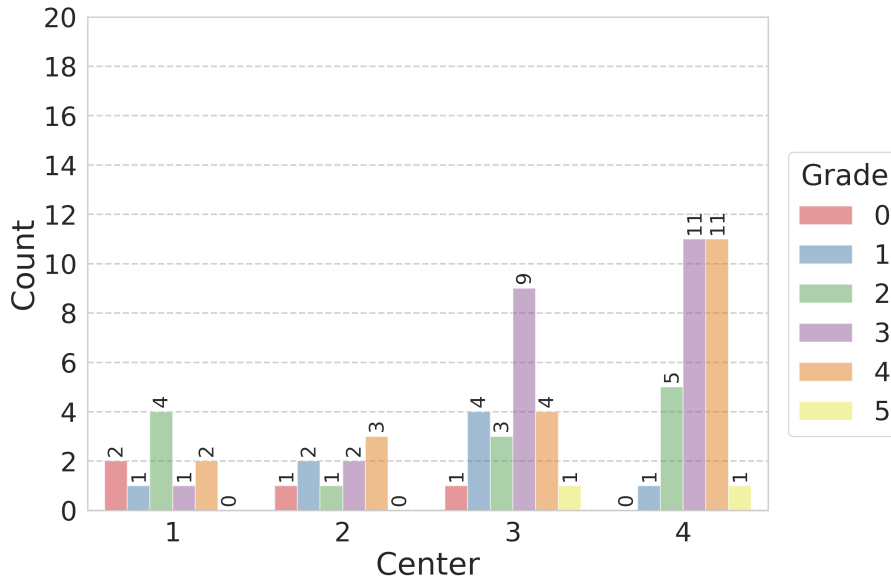
2.4. Assessment Methods

The evaluation of this challenge is based on two complementary metrics: the macro-averaged F1-score, also known as the Dice coefficient, and the Expected Cost (EC) with linear weights. Together, these metrics provide a robust assessment of model performance in a multi-class setting with ordinal structure.

¹Available at <https://nextcloud.tso.ukdd.de/s/XppWkRnWpLGwj5F> Password for Review: FedSurg24_data!



(a) Training Dataset Distribution.



(b) Testing Dataset Distribution.

Figure 2: **Label Distribution Across Data Subsets per Center.** Label distributions for (a) the training dataset and (b) the test dataset across the four centers. In the training set visualization, the darker segments represent the publicly available subset for participant development, while the lighter segments show the complete dataset used for final federated training. The plots highlight notable inter-center variability and class imbalance.

F1-score (Dice Coefficient):

The F1-score is widely used for balancing precision and recall, offering a harmonic mean that reflects both the accurate identification of relevant instances and the minimization of false positives [26, 27]. Given a confusion matrix $\mathbf{M} \in \mathbb{N}^{C \times C}$, where $M_{i,j}$ denotes the number of samples with ground-truth class i predicted as class j , the F1-score for class c is computed as:

$$\text{F1}_c = \frac{2 \cdot \text{TP}_c}{2 \cdot \text{TP}_c + \text{FP}_c + \text{FN}_c} \quad (1)$$

where:

$$\begin{aligned} \text{TP}_c &= M_{c,c} \quad (\text{true positives}) \\ \text{FP}_c &= \sum_{\substack{i=1 \\ i \neq c}}^C M_{i,c} \quad (\text{false positives}) \\ \text{FN}_c &= \sum_{\substack{j=1 \\ j \neq c}}^C M_{c,j} \quad (\text{false negatives}) \end{aligned}$$

The overall F1-score is calculated as the macro-average across all classes:

$$\text{F1}_{\text{macro}} = \frac{1}{C} \sum_{c=1}^C \text{F1}_c \quad (2)$$

Expected Cost (EC)

To account for the ordinal nature of the classification task, we also report the Expected Cost (EC), which penalizes misclassifications based on their severity. This aligns with the principle of ordinal monotonicity, where predictions farther from the ground-truth class incur higher penalties [28, 29, 27]. The EC is defined as:

$$\text{EC} = \frac{1}{N} \sum_{i=1}^C \sum_{j=1}^C M_{i,j} \cdot w_{i,j} \quad (3)$$

where:

$$\begin{aligned} N &= \sum_{i=1}^C \sum_{j=1}^C M_{i,j} \quad (\text{total number of samples}) \\ w_{i,j} &= \frac{|i-j|}{C-1} \quad (\text{cost of predicting class } j \text{ when the true class is } i) \end{aligned}$$

with the linear weight function:

$$w_{i,j} = \frac{|i-j|}{C-1} \quad (4)$$

This assigns zero cost to correct predictions and a linearly increasing penalty for deviations, with a maximum cost of 1 for the farthest misclassifications.

2.4.1. Ranking

To ensure a fair evaluation of submissions across both generalization and adaptation scenarios, we implemented a ranking framework that integrates multiple performance metrics with rigorous statistical analysis. Only submissions that successfully completed both tasks were considered. Teams failing to meet this criterion or submitting non-executable code were disqualified. Our ranking methodology guaranteed that models were evaluated not just on average performance but also on their robustness and consistency across heterogeneous data settings. The details of our evaluation procedure are described below.

For Task 1 (generalization), we computed the F1-score and the EC for all test cases. Separate rankings were assigned based on each metric, and a team’s overall rank for Task 1 was derived by averaging these two ranks. For Task 2 (adaptation), the metrics were first averaged across all three centers, and the same ranking scheme used in Task 1 was then applied.

The final leaderboard was determined by averaging each team’s ranks across both tasks, providing a comprehensive assessment of overall performance throughout the challenge.

Additionally, to ensure the robustness and reliability of the rankings, bootstrapping [30] was applied. Bootstrapping, as emphasized by Maier-Hein et al. [31], is a key method for assessing the variability of rankings and the stability of observed performance differences. In this study, the test set was repeatedly resampled with replacement for 10,000 iterations, and team rankings were recalculated for each resample. For each team, we computed the proportion of iterations in which it retained its original rank as well as the proportions in which it achieved each of the other possible ranks. To statistically compare team performances, we applied the Wilcoxon signed-rank test to the bootstrapped metric values obtained over all iterations, thereby quantifying whether observed performance differences were significant beyond random variation.

3. Results

The FedSurg challenge received 24 registrations, with four final submissions. However, one submission was disqualified due to non-executable code after the final deadline. This left three complete submissions for evaluation. The participating teams were: Santhi R. Kolamuri, who submitted independently as Team Santhi; Lorenzo Mazana and Claas de Boer from the Translational Surgical Oncology group at the National Center for Tumor Diseases, submitting as Team Elbflorenz; and Julia Alekseenko and Nicolas Padoy from the CAMMA research group at IHU Strasbourg, submitting as Team Camma. Furthermore, we provide centralized baseline and a federated Swarm Learning (SL) baseline.

3.1. Participating Teams and Methods

The following section details the methodologies submitted by participants in the FedSurg challenge. Each subsection outlines the architectural choices, training strategies, and FL configurations employed. Where relevant, we contextualize each approach within existing literature on foundation models, metric learning, and federated optimization. A summary of each submission is presented in Table 2.

3.1.1. Team Santhi

Santhi R. Kolamuri’s approach leverages a pretrained Video Vision Transformer (ViViT) [32], which is well-suited for capturing spatio-temporal features in surgical video sequences (Figure 3 (a)). ViViT’s transformer-based architecture has proven more effective than

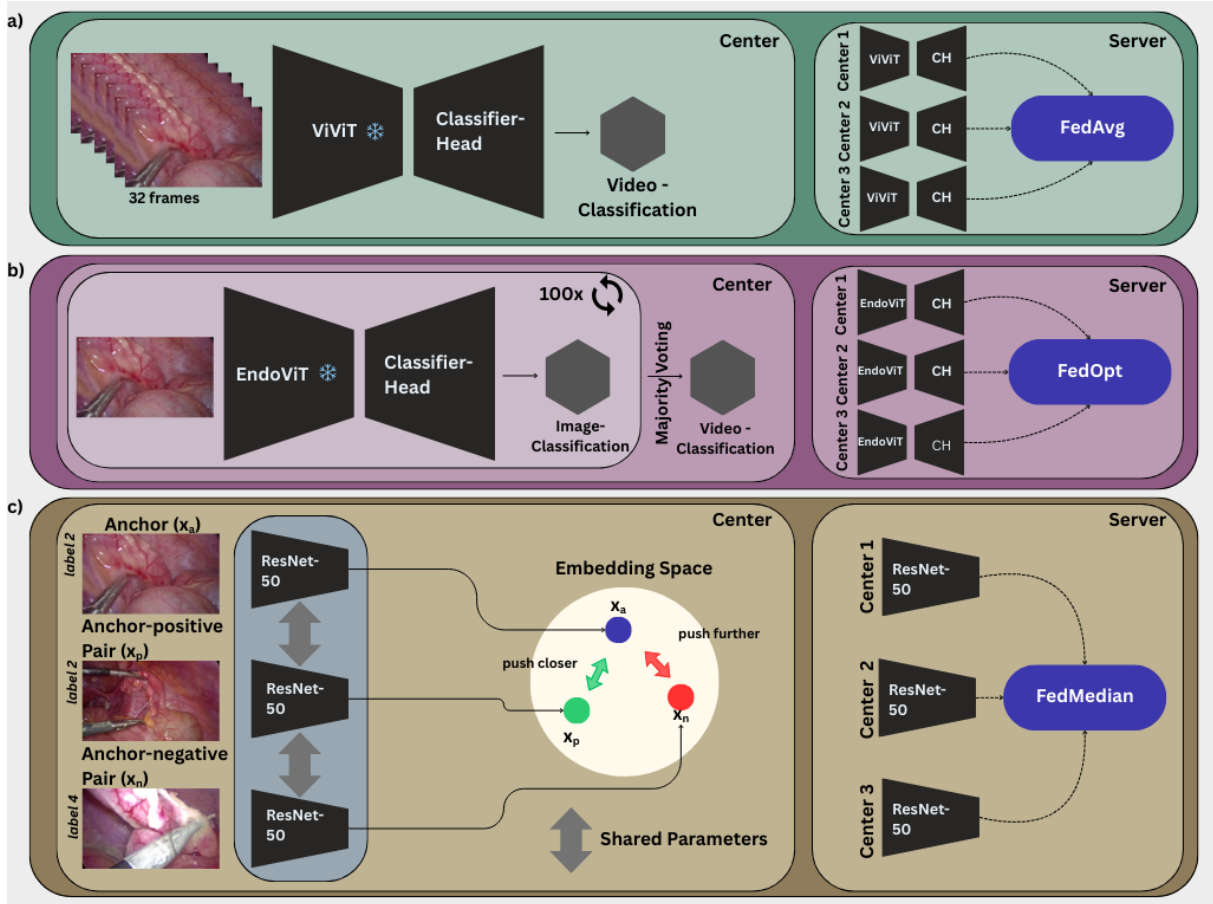


Figure 3: **Methods Overview:** The three submissions shown utilize different backbone architectures and federated strategies. A common approach is that in each server round, the best-performing model from a client’s local training rounds is sent to the server for aggregation. (a) Team Santhi uses a frozen ViViT backbone with a fine-tuned classification head processing 32 frames per video, with updates aggregated via FedAvg. (b) Team Elbflorenz uses a frozen EndoViT backbone with a fine-tuned head, predicting single frames repeatedly and combining them via majority voting, with updates aggregated via FedSAM. (c) Team Camma uses ResNet50 models trained with a contrastive approach on positive and negative pairs, with updates aggregated via FedMedian. At inference, classification is performed by comparing the test embedding to a support set.

Table 2: Overview of submissions to the FedSurg Challenge, detailing each team’s backbone model, prediction method, frame sampling, loss function, optimizer, learning rate, batch size, and federated learning configuration (FL strategy, FL-rounds, and local rounds).

| Team | Santhi | Elbflorenz | Camma |
|--------------------------|---|--|---|
| Backbone Model | Pretrained Video Vision Transformer (ViViT) with a frozen backbone. | Pretrained EndoViT with a frozen encoder. | Siamese network with a ResNet-50 backbone. |
| Prediction Method | Video-level classification. | Majority voting on independent frame-level classifications. | Compares test embedding to class prototypes or a full support set. |
| Frame Sampling | Samples 32 frames, with two-thirds from a narrow window around the center and the rest from the full sequence with a bias towards the center. | Uses 100 equidistant frames from each video. | Selects representative frames based on cosine similarity to a reference embedding, plus the central keyframe. |
| Loss Function | Cross-entropy loss. | Weighted cross-entropy loss to address class imbalance. | Triplet margin loss with cosine similarity. |
| FL Strategy | Federated Averaging (FedAvg). | Adaptive Federated Sharpness-Aware Minimization (FedSAM) on Client-side and FedOpt on Server Side. | Federated Median (FedMedian). |
| Optimizer | Adam | adaptive Federated Sharpness Aware Minimization (FedSAM) based on SGD | Adam |
| FL-Rounds | 5 | 50 | 10 |
| Local Rounds | 20 | 2 | 5 |
| Learning Rate | 1×10^{-4} | 1×10^{-3} | 1×10^{-6} |
| Batchsize | 4 | 128 | 1 |

conventional CNNs in modeling temporal dependencies. By utilizing ViViT pretrained on Kinetics-400, only the final classification layer is fine-tuned, while all other weights remain frozen. This linear probing approach is common for foundation models [33], as it allows efficient adaptation while retaining robust pretrained representations.

The frame loading strategy is customized to emphasize salient temporal regions. From 200 available video frames, 32 are sampled for training. Two-thirds are selected from a narrow window around frame 100 to capture high-information segments, while the remainder of the frames are drawn from the full sequence with 60% probability to the frames near the center. This hybrid sampling balances local relevance and temporal diversity.

Training is implemented via the Flower FL framework [34], using FedAvg for aggregation. Centers train locally with a batch size of four for five epochs per round, across 20 communication rounds. Cross-entropy loss is used with mixed precision training to improve memory efficiency. The lightweight design, frozen backbone, focused sampling, and shallow head enable fast convergence with low resource demands. This submission builds on the success of ViViT in centralized video classification while adapting it to the constraints of FL.

3.1.2. Team *Elbflorenz*

Team *Elbflorenz* adopts a foundation model-based strategy using EndoViT [35], a Vision Transformer pretrained on the Endo700k dataset consisting of diverse endoscopic images (Figure 3 (b)). Following a standard linear probing setup [33], the encoder is frozen and only a lightweight classification head is trained. This setup is motivated by recent successes of foundation models in medical imaging [36, 37], where pretrained encoders generalize well even with limited task-specific data.

The model uses 100 equidistant frames from each video and independently classifies each frame. A weighted cross-entropy loss is used to mitigate class imbalance, with weights inversely proportional to class frequency. Final video-level predictions are determined via majority voting. In the event of a tie, average confidence scores guide the decision. This per-frame classification strategy increases robustness by aggregating multiple frame-level predictions.

Federated optimization on the client side is handled using adaptive FedSAM [38, 39], which extends Sharpness-Aware Minimization (SAM) to heterogeneous FL settings. This method encourages flatter minima and better generalization across non-IID (independent and identically distributed) client data. Similar to Team *Santhi*'s approach, training was implemented via the Flower FL framework [34]. It employs 2 local epochs and 50 global rounds, with center-side class balancing and hyperparameter tuning. Compared to standard FedAvg, FedSAM has demonstrated improved convergence on non-IID data [38]. Model aggregation on the server is done with FedOpt [40]. By combining EndoViT with adaptive optimization, Team *Elbflorenz* presents a minimal yet effective pipeline for surgical appendicitis classification under federated constraints.

3.1.3. Team *Camma*

Team *Camma* employs a metric learning approach based on a Siamese network with a ResNet-50 backbone [41], inspired by the original Siamese architecture [42]. Unlike conventional classifiers that output class probabilities, this model maps input images to L2-normalized 256-dimensional embeddings. Training is performed using triplet margin loss with cosine similarity, encouraging embeddings from the same appendicitis stage to cluster while pushing apart those from different stages (Figure 3 (c)).

At inference, classification is performed by comparing the test embedding to a support set. This is done either via class prototypes (mean embeddings) or by averaging distances to all embeddings within each class. Camma observed that prototype-based inference worked best for Centers 2 and 3, while per-sample comparison was more effective for Center 1, allowing the approach to flexibly adapt to center-specific data distributions.

This metric learning paradigm is particularly well-suited for FL, as it focuses on learning a robust embedding space rather than simply aggregating classifier weights, which can be highly sensitive to the non-independent-and-identically-distributed (non-IID) label distributions across centers.

To address domain heterogeneity, the model incorporates Switchable Normalization [43], which combines batch, instance, and layer normalization through softmax gating. This adaptive scheme enhances generalization across diverse centers, which is crucial in federated settings.

In addition, frame selection leverages embedding-based similarity: representative frames are chosen based on cosine similarity to a ResNet-50 reference embedding, alongside the keyframe (frame 100), to improve input consistency.

Training is conducted within a custom FL framework using the FedMedian aggregation strategy [10], which is robust to outliers. Each center performs 10 local epochs followed by 5 epochs dedicated to triplet optimization. The locally best-performing model (by F1-score) is selected for aggregation, ensuring only high-quality updates contribute to the global model. Overall, Team Camma’s method demonstrates how metric learning, adaptive normalization, and robust aggregation can be combined for scalable, personalized FL in surgical video classification.

3.2. Baselines

In addition to the three participating teams, we provide two baselines for comparison: a centralized baseline and a federated baseline. Both baselines are based on the SurgTempoNet method [22].

SurgTempoNet employs a spatial-temporal architecture designed to predict patient-level clinical outcomes directly from laparoscopic videos. The model utilizes a ConvNeXt-Base [44] backbone, pre-trained on ImageNet-22k [45], to extract high-level feature representations from individual frames. In its temporal configuration, these features are fed into a single-layer Long Short-Term Memory (LSTM) [46] network with a hidden state size of 160. This allows the model to aggregate sequential information across the entire surgical procedure, mapping a sequence of frames to a single global label through a final linear classification layer.

To manage the high dimensionality of surgical footage, the pipeline uses a weakly supervised approach with sparse frame sampling. Videos are processed at a rate of one frame per second, and frames are resized to a resolution of 480×270 pixels. This sampling strategy reduces the computational burden of processing every raw video frame.

Both centralized and federated training is conducted using the AdamW optimizer with a learning rate of 1.0×10^{-3} . To address the inherent class imbalance in surgical datasets, the model utilizes Weighted Cross-Entropy Loss, where weights are inversely proportional to the frequency of each disease stage in the training set. Furthermore, a batch accumulation strategy is implemented, where gradients are computed over mini-batches of 64 clips, but weights are updated only every three steps, effectively stabilizing the training process for video sequences.

The defining characteristic of the federated baseline is its integration into an SL framework [47, 48]. Unlike centralized training or standard FL, local models are trained on

site-specific data, and only the model weights are synchronized via a peer-to-peer network managed by a SwarmCallback function. This synchronization occurs at a fixed frequency (e.g., every 100 batches) and requires a minimum number of active peers to proceed.

Furthermore, to probe whether parameter-efficient fine-tuning (PEFT) constitutes a viable adaptation strategy in this data regime, two additional preliminary models are included. Both apply Low Rank Adaptation (LoRA) [49] (rank 8, alpha 16) to the attention projections of a frozen backbone, combined with a shared three-layer MLP classification head and FedAvg aggregation over 25 rounds; all remaining hyperparameters (ASAM optimizer, cosine annealing, four local epochs per round) are held constant.

The *EndoViT+LoRA* baseline builds on the Team Elbflorenz architecture, adapting the frame-level EndoViT backbone [35] (ViT-Base, pretrained on endoscopic image data; $\sim 940\text{K}$ trainable parameters) with single-frame inputs (224×224). The *ViViT+LoRA* baseline extends this to temporal modeling by substituting a ViViT-B-16 \times 2 backbone pretrained on Kinetics-400, processing 16-frame clips through native spatial-temporal attention ($\sim 969\text{K}$ trainable parameters), following the architectural principle of Team Santhi. Both baselines are post-hoc organizer analyses and are not part of the official challenge ranking.

3.3. Scores and Rankings

The performance of the submitted federated models was evaluated in both tasks of the FedSurg Challenge: generalization to an unseen center (Task 1) and center-specific adaptation (Task 2). Performance was measured using EC and F1-score. Rank stability was assessed via 10,000-iteration bootstrapping, followed by the Wilcoxon signed-rank test for statistical significance. Additionally, the baseline methods are reported separately in Section 3.4 as contextual references and are not part of the official challenge ranking. Overall, a comprehensive summary of results, including key metrics, confusion matrices, and rank stability, is provided in Tables 3 and 4 and Figures 4, 5, 6, and 7, with further details in Appendix G.

3.3.1. Task 1: Generalization to an Unseen Center

Table 3: Performance comparison of the three teams on Task 1 at the held-out center (Center 4), reporting Expected Cost (EC, lower is better) and F1-score (higher is better). Best results are highlighted in bold.

| Team | EC \downarrow | F1 \uparrow |
|------------|-----------------|---------------|
| Camma | 57.24% | 4.76% |
| Elbflorenz | 24.14% | 7.83% |
| Santhi | 12.41% | 23.03% |

Task 1 assessed the models’ ability to generalize to Center 4, which was excluded during training. Overall, performance on this task was modest across all teams (Table 3).

Team Santhi achieved the highest F1-score (23.03%) and the lowest EC (12.41%), demonstrating superior generalization under domain shift. This is evident in the confusion matrix (Figure 4), where Santhi’s predictions tend to align with the diagonal, in contrast to the predictions heavily biased towards a specific class. The model correctly identified class 3 in 8 out of 11 cases but struggled with adjacent stages (e.g., classes 2 and 4) and underrepresented ones (e.g., 0, 1, 5), likely due to class imbalance. Bootstrapped performance metrics (Figure 5) confirm the statistical robustness of these findings. This is further supported by the ranking stability plots (Figures 6a and 6b), where Team Santhi ranks first in 99.23% of bootstrapped samples for F1-score and 99.79% for EC.

Confusion Matrices – Task 1 (Center 4)

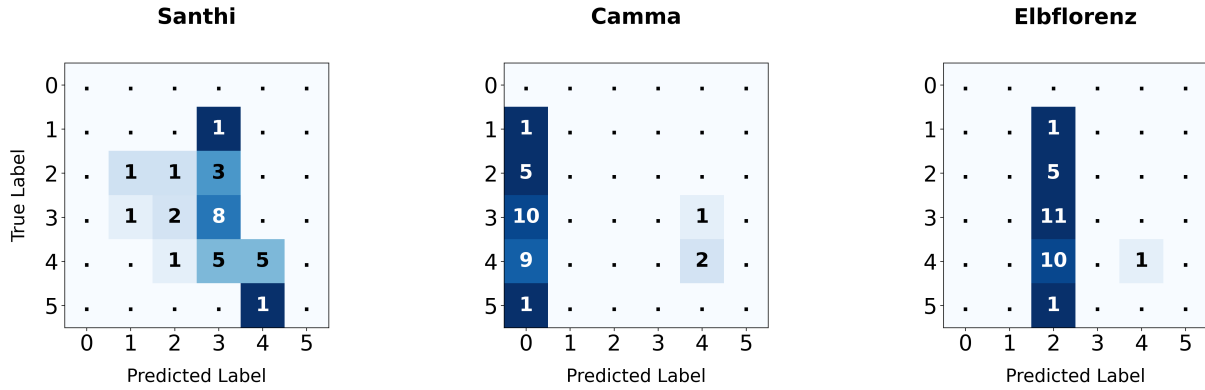


Figure 4: **Confusion Matrices – Task 1, Center 4.** Confusion matrices for the participating teams on Center 4 (Task 1). The values in the confusion matrices are not normalized. The color highlighting is normalized row-wise by true labels. The diagonal highlights class-wise recall, while off-diagonal values indicate common misclassification patterns.

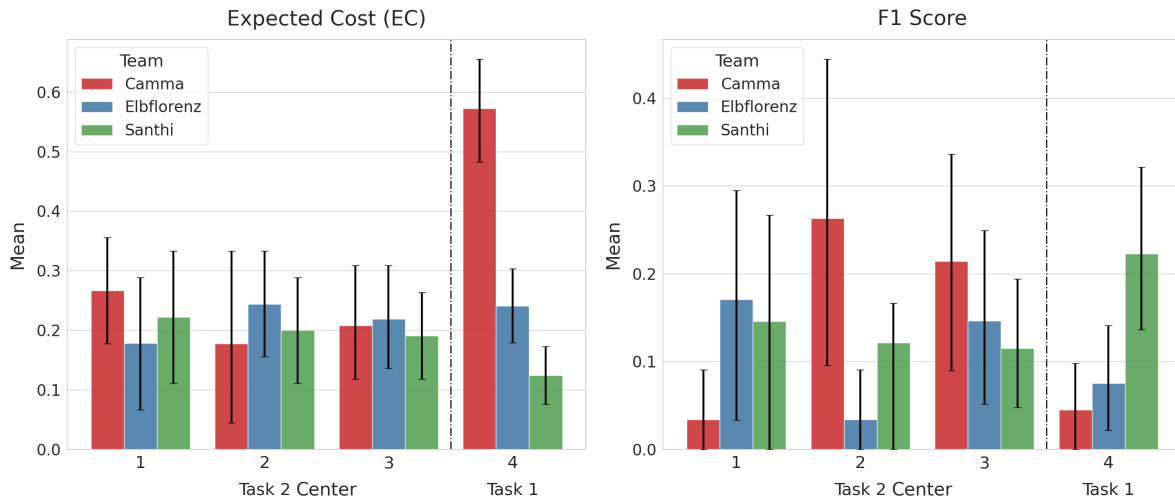


Figure 5: **Bootstrapped Performance Results.** Visualization of the performance results with standard deviation as error bars for all teams and tasks after bootstrapping with 10,000 repetitions. The plot illustrates the variability and stability of the outcomes across different centers.

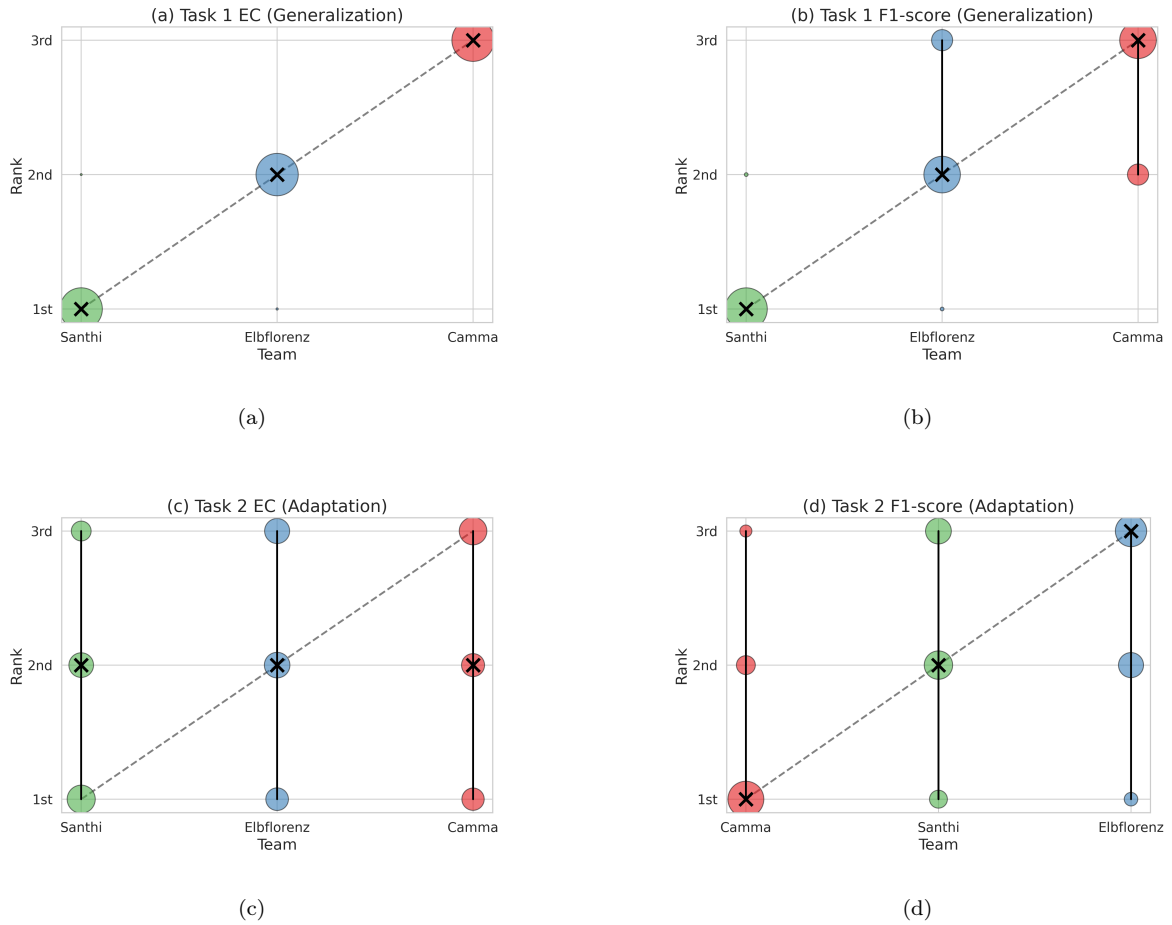


Figure 6: **Ranking Stability.** Bootstrapped ranking distributions for each metric and task, based on 10,000 bootstrap iterations. Circle size indicates the percentage of times a team’s model achieved a specific rank across samples. Black crosses show median ranks, and black lines denote the 95% bootstrap confidence intervals. Subfigures (a) and (b) correspond to Task 1 (generalization ability) with metrics EC and F1-score, respectively, while (c) and (d) represent Task 2 (adaptation ability) using the same metrics.

Team Camma obtained the lowest F1-score (4.76%) and the highest EC (57.24%). The model predominantly predicted class 0, achieving only three correct predictions across the dataset. This behavior indicates a failure to generalize, likely caused by the model overfitting to the training distribution and being unable to adapt to the significant domain shift in the unseen test set. The poor performance of this trivial classifier is supported by bootstrapping analysis (Figure 5) and statistical significance testing (Table 3). Across 10,000 repetitions, Team Camma consistently ranked as the lowest-performing team in 100% of cases for the EC and 75.09% for the F1-score (Figure 6).

Team Elbflorenz also demonstrated limited performance, predominantly predicting class 2 across inputs (Figure 4). The model achieved an EC of 24.14% and an F1-score of 7.83%, ranking slightly above Team Camma. This is likely due to the classifier exhibiting a strong bias towards predicting classes adjacent to the most frequently observed labels in the training data. Confusion matrices and bootstrapped scores confirm weak generalization, placing Elbflorenz in the middle of the three submissions in terms of overall performance (Figure 6, Figure 5).

Wilcoxon signed-rank tests confirmed statistically significant performance differences between all models at Center 4. This validates that the observed variations in EC and F1-score reflect meaningful distinctions in generalization ability under domain shift. The ranking stability plot (Figure 6) visually reinforces this trend, clearly showing Team Santhi in the lead, followed by Elbflorenz and Camma. Therefore, the leaderboard presented in Table 5 is robust.

3.3.2. Task 2: Center-Specific Adaptation

Table 4: Performance comparison of the three teams on Task 2 across Centers 1, 2, and 3. The table reports Expected Cost (EC, lower is better) and F1-score (higher is better). Best results per metric and center are highlighted in bold.

| Team | Center | EC ↓ | F1 ↑ |
|------------|---------|---------------|---------------|
| Camma | | 26.67% | 3.70% |
| Elbflorenz | 1 | 17.78% | 20.20% |
| Santhi | | 22.22% | 20.83% |
| Camma | | 17.78% | 30.28% |
| Elbflorenz | 2 | 24.44% | 3.70% |
| Santhi | | 20.00% | 13.33% |
| Camma | | 20.91% | 22.76% |
| Elbflorenz | 3 | 21.82% | 15.51% |
| Santhi | | 19.09% | 12.04% |
| Camma | | 21.79% | 18.91% |
| Elbflorenz | Average | 21.35% | 13.14% |
| Santhi | | 20.44% | 15.40% |

Task 2 evaluated model performance in intra-center settings, where each local model was tested on its dedicated test set from its associated center. All teams demonstrated improvements over Task 1, although performance varied considerably across centers (Table 4, Figure 5).

Team Santhi demonstrated robust performance across centers, with F1-scores of 20.83% (Center 1), 13.33% (Center 2), and 12.04% (Center 3) (Table 4). Although not consistently the best at individual centers, their steady results, combined with relatively low

Confusion Matrices – Task 2 (Centers 1-3)

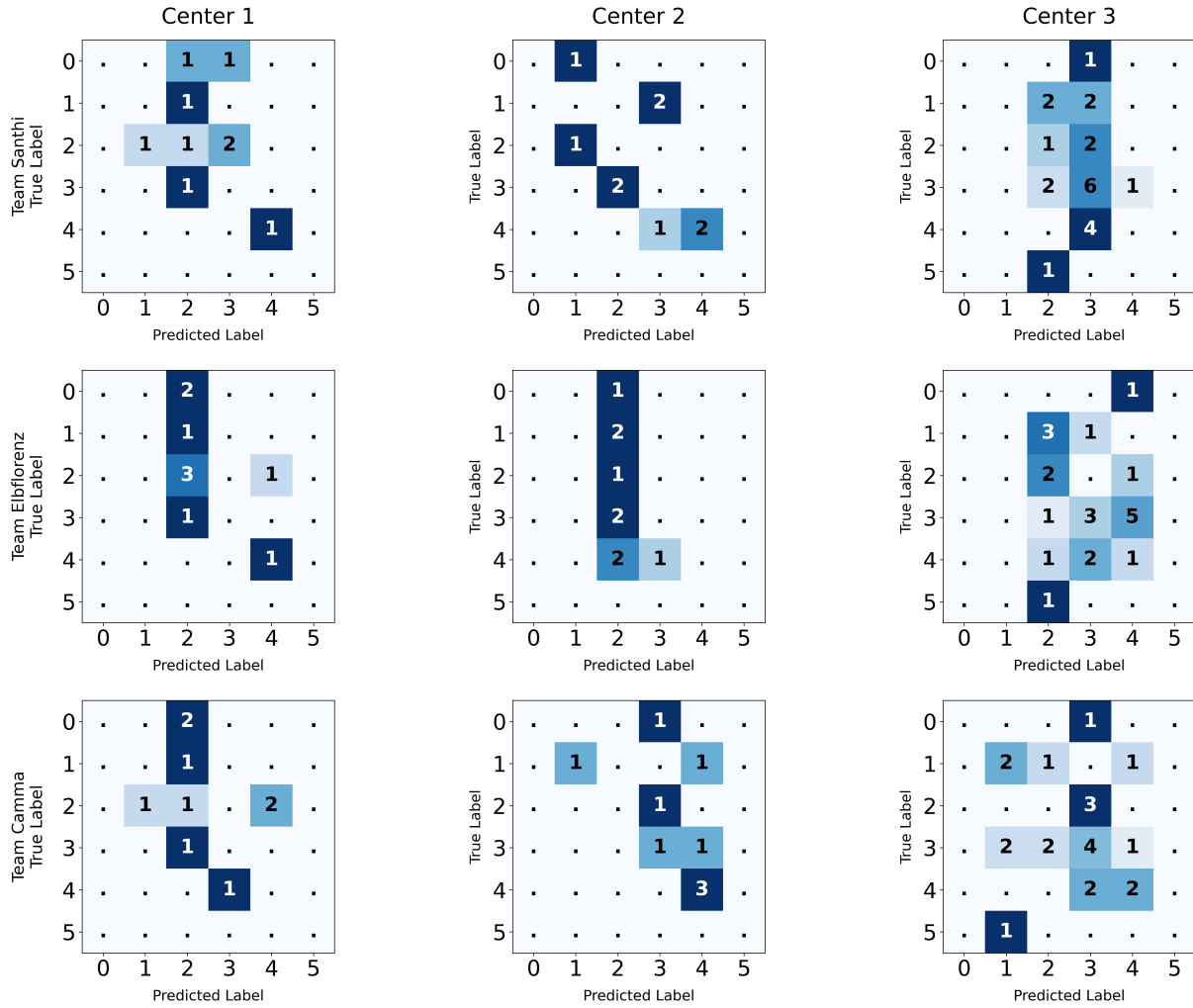


Figure 7: **Confusion Matrices – Task 2, Centers 1–3.** The values in the confusion matrices are not normalized. The color highlighting is normalized row-wise by true labels. The diagonal highlights class-wise recall, while off-diagonal values indicate common misclassification patterns.

EC values, indicate effective regularization and strong adaptability to the test data of the training centers. The confusion matrices in Figure 7 reveal predictions largely concentrated along the diagonal, suggesting good class differentiation. In Center 3, however, the local model, similar to Team Elbflorenz, showed limited discriminatory power, with a tendency to predict classes 2, 3, or 4 rather than providing balanced classification. Bootstrapping analysis (Figure 5) confirms consistent performance across centers, but the final ranking remained unstable, as indicated by the wide 95% confidence intervals in Figure 6. For the F1-score, Santhi ranked first in 17.86% of iterations, second in 45.02%, and third in 37.12%; for EC, the respective values were 44.12%, 33.94%, and 21.94%.

Team Elbflorenz displayed greater inconsistency across centers, especially in the F1-score (Figure 5). The confusion matrices (Figure 7) reveal inconsistent local adaptation: the models for Centers 1 and 2 collapsed into trivial classifiers, biasing predictions towards a single class, while the model for Center 3 failed to discriminate effectively between classes 2, 3, and 4. Despite this, the model performed relatively well at Center 1 (F1: 20.20%), but performance dropped markedly at Center 2 (3.70%) and moderately at Center 3 (15.51%). Bootstrapping results suggest difficulties in achieving reliable within-center generalization, potentially attributable to data imbalance or overfitting. Similar to Team Santhi, Team Elbflorenz’s ranking fluctuates between first, second, and third place across evaluation metrics (Figure 6). For the F1-score, Elbflorenz ranked first in 10.23% of cases, second in 35.03%, and third in 54.74%. Regarding the EC metric, Elbflorenz achieved first place in 44.12% of cases, second place in 33.94%, and third place in 21.94%.

Team Camma exhibited pronounced center-dependent performance (Table 4, Figure 5), excelling at Center 2 with an F1-score of 30.28% and at Center 3 with 22.76%, but underperforming significantly at Center 1, where the F1-score was 3.70%. Confusion matrices shown in Figure 7 indicate intermediate performance relative to Teams Santhi and Elbflorenz, as the models demonstrate a modest ability to differentiate between classes, evidenced by a visible diagonal tendency. Similar to the other submissions, bootstrapping analyses confirm variability in performance across centers. The ranking for Team Camma also fluctuates across centers, with F1-score rankings of 1st place in 71.29% of cases, 2nd place in 19.94%, and 3rd place in 8.14%. For the EC metric, the rankings were 1st place in 27.81%, 2nd place in 29.55%, and 3rd place in 42.64%.

Importantly, Wilcoxon signed-rank tests revealed statistically significant performance differences between the models for all centers and both metrics. Conducting the test after bootstrapping substantially supports the statistical power, ensuring that the detected differences were not due to chance. Despite these significant differences, the bootstrapped ranking stability analysis (Figures 6c and 6d) shows notable fluctuations in team positions within the bootstrapping. While the Task 2 F1-score rankings (Figure 6d) align with the overall standings in Table 5, the EC mean-based rankings (Figure 6c) reveal no clear winner with respect to the median rank. Nevertheless, the frequency of rank positions matches the trend of the general ranking in Table 5. Such variability highlights that Task 2 outcomes are sensitive to small changes in the test set, and claims regarding top-performing submissions should therefore be made with caution. In line with the interpretation of Maier-Hein et al. [31], the fact that no team retained its original EC rank in at least 50% of bootstrap replicates indicates that the Task 2 ranking is unstable. We therefore report the original ranking for completeness, while emphasizing that it should not be interpreted as conclusive evidence of submission superiority.

Table 5: Team rankings for the FedSurg Challenge are presented, where lower ranks indicate better performance.

| Team | Task 1 Ranks | | | Task 2 Ranks | | | Final Rank |
|------------|--------------|----------|-----|--------------|----------|-----|------------|
| | EC | F1-score | Avg | EC | F1-score | Avg | |
| Camma | 3 | 3 | 3 | 3 | 1 | 2 | 2 |
| Elbflorenz | 2 | 2 | 2 | 2 | 3 | 3 | 2 |
| Santhi | 1 | 1 | 1 | 1 | 2 | 1 | 1 |

3.4. Further Analysis

Challenge participant results are compared against organizer-provided baselines comprising centralized training, SL, and parameter-efficient fine-tuning (PEFT) variants to disentangle intrinsic task difficulty from federated overhead. Communication efficiency across all evaluated approaches is analyzed subsequently. Ranking and evaluation methodology are described in Section 2.4.1.

3.4.1. Baseline comparison

Table 6: Absolute raw test performance comparison including baselines. EC: lower is better; F1: higher is better. Baseline rows in the lower half of the table are contextual references and are not part of the official challenge ranking.

| Method | Task 1 EC | Task 1 F1 | Task 2 Avg EC | Task 2 Avg F1 |
|--------------|---------------|---------------|---------------|---------------|
| Camma | 57.24% | 4.76% | 21.79% | 18.91% |
| Elbflorenz | 24.14% | 7.83% | 21.35% | 13.14% |
| Santhi | 12.41% | 23.03% | 20.44% | 15.40% |
| Cen | 10.34% | 26.31% | 19.82% | 23.51% |
| SWARM | 13.10% | 19.00% | 20.41% | 17.77% |
| EndoViT+LoRA | 17.24% | 9.24% | 20.13% | 8.70% |
| ViViT+LoRA | 22.76% | 15.93% | 17.60% | 21.47% |

Table 7: Center-wise Task 2 baseline results. EC: lower is better; F1: higher is better.

| Baseline | Center 1 | | Center 2 | | Center 3 | |
|--------------|----------|--------|----------|--------|----------|--------|
| | EC | F1 | EC | F1 | EC | F1 |
| Cen | 24.00% | 11.43% | 20.00% | 26.43% | 15.45% | 32.67% |
| SWARM | 28.00% | 10.32% | 17.78% | 20.95% | 15.45% | 22.03% |
| EndoViT+LoRA | 17.78% | 10.32% | 24.44% | 6.06% | 18.18% | 9.68% |
| ViViT+LoRA | 22.22% | 12.22% | 13.33% | 22.62% | 17.27% | 29.57% |

To provide a comprehensive benchmark, we introduced four baselines. A centralized (Cen) baseline, representing the upper bound of performance by training on pooled data from all centers for Task 1 and on each center’s data separately for Task 2, and an SL baseline, applying the same architecture in a decentralized peer-to-peer (P2P) setup, together quantify the cost of decentralization. Two additional PEFT baselines, EndoViT+LoRA and ViViT+LoRA, probe whether parameter-efficient adaptation can serve as a practical alternative to full local fine-tuning. Table 6 summarizes absolute raw test performance across both tasks, while Table 7 reports center-wise Task 2 results for all baseline models.

Comparative Performance. The centralized baseline outperformed all decentralized models in both tasks, achieving the top rank in both F1-score and EC metrics. In Task 1 (Generalization), the centralized baseline reached an F1-score of 26.31% and an EC of 10.34%, followed by Santhi and the SL baseline (compare Figure 9). Camma and Elbflorenz recorded the lowest Task 1 performance among all methods, with F1-scores of 4.76% and 7.83% respectively.

In Task 2 (Adaptation), the performance gap narrowed, reflecting the challenge of center-specific fine-tuning. While the centralized model maintained the lead (Avg. F1: 23.51%), the SL baseline demonstrated strong adaptation across the three centers, securing the second overall rank for this task besides Santhi’s method (compare Table H.11). Camma and Elbflorenz both improved substantially in Task 2 relative to their Task 1 performance, yet neither reached the performance level of the centralized or SL baselines.

The two PEFT baselines reveal a clear separation by architecture. EndoViT+LoRA achieved 9.24% F1 on Task 1 and only 8.70% average F1 on Task 2, performing comparably to Elbflorenz, the frame-level method it is derived from, but failing to surpass it. Inspection of per-class predictions confirms near-complete collapse to the majority class, indicating that LoRA adaptation of a frame-level backbone is insufficient to overcome the high intra-video visual variance at an unseen center. ViViT+LoRA, by contrast, achieved 15.93% F1 on Task 1 and 21.47% average F1 on Task 2, ranking second among all methods in Task 2. Notably, at Center 3, ViViT+LoRA reached 29.57% F1, the highest Task 2 F1 among all non-centralized methods and approaching the centralized baseline (32.67%). Performance at the smaller centers remained limited (Center 1: 12.22%, Center 2: 22.62%), consistent with the quantity-skew effect described in Section 4.3: local adaptation via PEFT benefits from sufficient local samples and is most effective at the largest node.

Rank Stability and Statistical Significance. To address the stability of these findings beyond point estimates, we conducted a stability analysis using 10,000-iteration bootstrapping. This process quantifies the probability of each team achieving a specific rank under different data distributions, as visualized in Figure 9.

As shown in Figure 9(a) and (b), the rankings for Task 1 were highly stable with a tendency to solve the ties in the ranking. For the F1-score, the centralized baseline retained the 1st rank in 67.0% of iterations, while SWARM maintained the 3rd rank in 72.7% of cases. In contrast, Task 2 exhibited higher volatility (Figure 9(c) and (d)), particularly in the EC metric. For instance, Camma’s rank for Task 2 EC was distributed across all five positions (retaining the 5th rank in only 31.9% of iterations), reflecting a higher sensitivity to the specific data composition of the adaptation centers.

The statistical significance of these rankings was validated using the Wilcoxon signed-rank test. In Task 1, all pairwise comparisons for both metrics yielded $p < 0.001$, indicating that the performance tiers between the baselines and participants are statistically distinct. In Task 2, while most differences remained highly significant ($p \approx 0$), the comparison between Santhi and SWARM for the EC metric yielded a p -value of 0.745. This suggests that their adaptation performance regarding surgical count estimation was statistically indistinguishable, despite their divergence in F1-score ($p < 0.001$).

The variability of these outcomes is further illustrated in Figure 8, where error bars represent the standard deviation across bootstrap replicates. The narrower distributions for Task 1 compared to the wider variance in Task 2 underscore the inherent difficulty of the adaptation task, where local center characteristics significantly influence model stability.

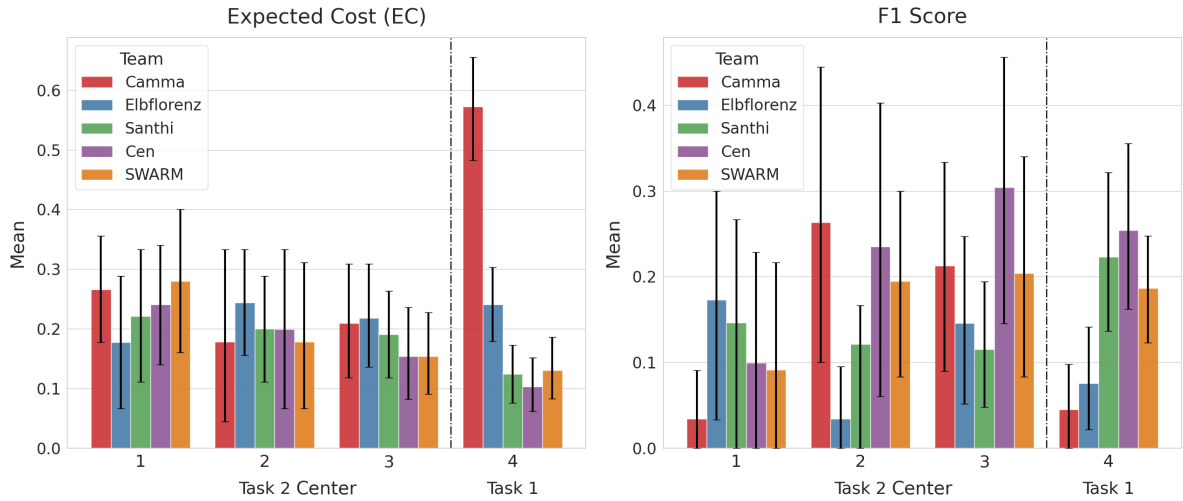


Figure 8: **Bootstrapped Performance Results with Baselines.** Visualization of the performance results with standard deviation as error bars for all teams and tasks after bootstrapping with 10,000 repetitions. The plot illustrates the variability and stability of the outcomes across different centers.

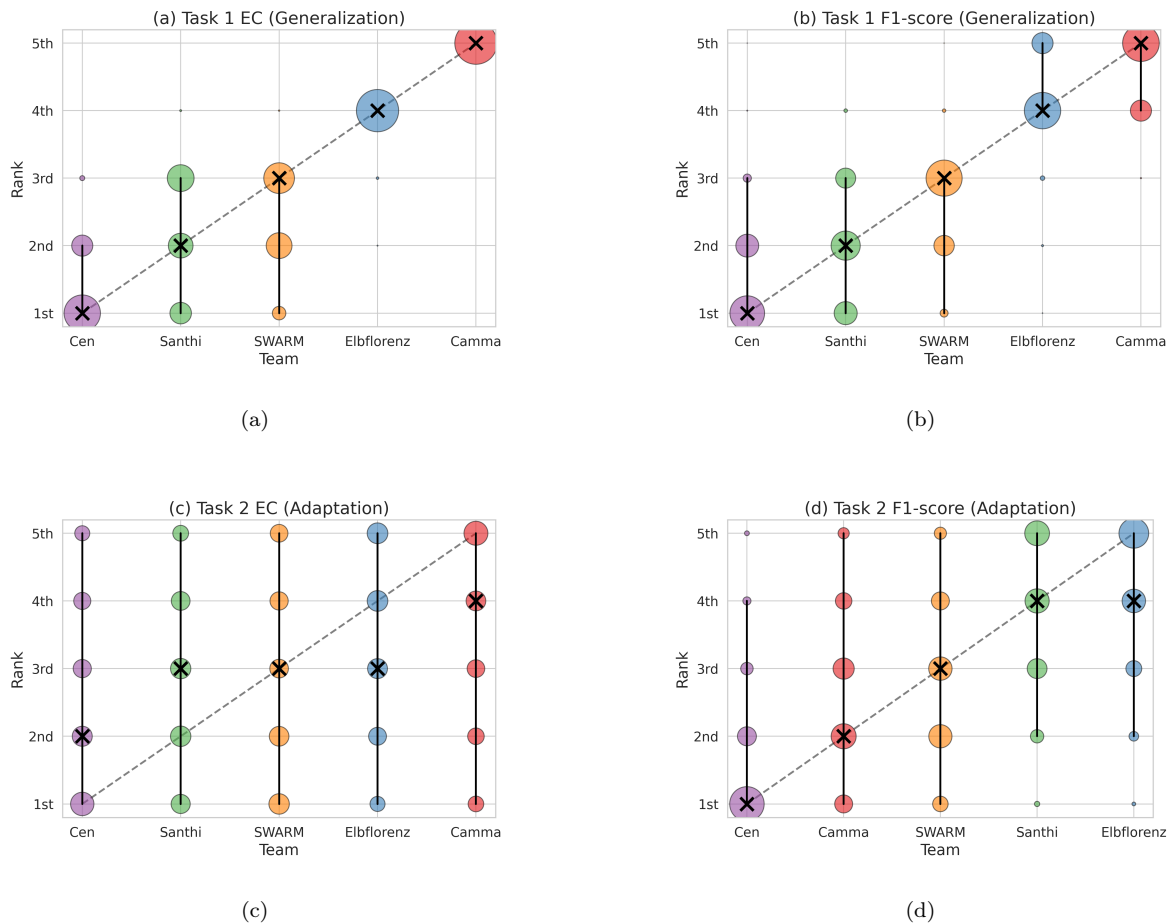


Figure 9: **Ranking Stability.** Bootstrapped ranking distributions for each metric and task, based on 10,000 bootstrap iterations. Circle size indicates the percentage of times a team’s model achieved a specific rank across samples. Black crosses show median ranks, and black lines denote the 95% bootstrap confidence intervals. Subfigures (a) and (b) correspond to Task 1 (generalization ability) with metrics EC and F1-score, respectively, while (c) and (d) represent Task 2 (adaptation ability) using the same metrics.

3.4.2. Communication efficiency analysis

Communication cost is a critical metric in decentralized machine learning because the frequent transmission of high-dimensional model parameters, weights, or gradients over limited or unstable network bandwidth can become a significant bottleneck [9]. In many medical AI applications, the time required for network synchronization often dwarfs the time spent on local GPU computation. Consequently, optimizing these costs is essential for making collaborative learning scalable and practical for real-world clinical scenarios.

In a traditional FL architecture, the total communication costs can be calculated using the following formula:

$$C_{\text{total}} = 2 \times K \times T \times |W| \quad (5)$$

Where:

- C_{total} is the total communication cost (data transferred).
- The factor of 2 accounts for the bi-directional transfer (upload and download) of model parameters between the client and the central server in each round.
- K is the number of participating clients (or nodes) per round.
- T is the total number of communication rounds.
- $|W|$ represents the size of the model parameters or weights.

However, for SL, the communication cost is calculated differently due to its peer-to-peer (P2P) nature. Since a central server does not exist, nodes synchronize weights directly through a decentralized mesh. In a leader-based synchronization (as utilized in the SurgTempoNet framework), one node is elected to aggregate weights from its peers. Consequently, the communication cost formula is adjusted to reflect the $K - 1$ active connections:

$$C_{\text{total}} = 2 \times (K - 1) \times S \times |W| \quad (6)$$

Where S represents the total number of synchronization events across the entire training duration. In the SurgTempoNet implementation, synchronization is governed by a frequency parameter rather than fixed rounds. The total number of synchronization events S for a node is defined as:

$$S = \sum_{n=i}^K \left\lfloor \frac{E \times B_i}{f_{\text{sync}}} \right\rfloor + 1 \quad (7)$$

Where:

- E is the number of local epochs performed.
- B_i is the number of batches contained in each epoch for center i .
- f_{sync} is the synchronization frequency (e.g., every 100 batches).
- The +1 accounts for the initial synchronization at the start of training.

By utilizing $2(K - 1)$, the model accounts for the fact that the aggregating node does not incur external network traffic for its own local weights. This provides a more rigorous representation of the physical network traffic generated during the decentralized training of surgical video classifiers across heterogeneous hospital sites.

Table 8 reveals again significant variance in both architectural complexity and the resulting communication overhead during the FL process.

Model Architecture and Parameterization. The models utilized by Santhi, Elbflorenz, and our SL Baseline share a similar scale, ranging around 88M parameters. In contrast, team Camma implemented a significantly more compact architecture. With only 24M parameters, Camma’s model is approximately 73 % smaller than the other methods. All models utilize 32-bit floating-point precision, resulting in a model size of approximately 340 MB for the larger architectures and around 92 MB for Camma’s compact model.

Synchronization Events and Total Communication Costs. As discussed, the total communication cost is a function of both the model size and the frequency of synchronization events. The SL Baseline, with its high synchronization frequency (100 events), incurs the highest communication cost, totaling approximately 133.14 GB across all clients and rounds, despite saving communication compared to the other methods by using a P2P approach. Furthermore, the impact of synchronization frequency is most evident when comparing Santhi and Elbflorenz.

Team Elbflorenz, with 50 synchronization events, results in a total cost of around 97.47 GB. Team Santhi, with only 20 synchronization events, significantly reduces the communication overhead to approximately 39.63 GB.

Finally, team Camma, with the smallest model and lowest synchronization frequency (10 events), achieves the lowest communication cost of about 5.38 GB.

In summary, team Camma emerged as the most communication-efficient team by a wide margin. By combining a reduced parameter count with a highly conservative synchronization strategy (10 sync events), they achieved a total communication cost of only 5.38 GB. Compared to the SL Baseline, this represents a 95.9% reduction in network traffic, highlighting the efficacy of aggressive model compression and sparse synchronization in federated environments.

In the current implementation, both PEFT baselines transmitted full model snapshots during aggregation, incurring communication costs comparable to full-model FL methods. Since only the LoRA adapter weights differ between federation rounds ($\sim 940\text{--}969\text{K}$ parameters, ~ 3.8 MB per model), a dedicated LoRA-only synchronization strategy would reduce per-round transmission to less than 2% of the costs reported in Table 8. This efficiency advantage was not exploited here, but represents a compelling practical benefit of PEFT-based FL for future implementations.

4. Discussion

The FedSurg challenge should be understood as a proof-of-concept benchmark: the appendectomy task was selected for its methodological tractability rather than for its immediate clinical impact. It offers a standardized surgical workflow, multi-center data availability, and an established grading system. The following discussion focuses on methodological insights transferable to future FL applications on surgical video, structured around two central questions: first, what architectural and algorithmic choices best support global generalization to unseen centers; and second, whether and how local adaptation can be reliably achieved without sacrificing the globally learned representation.

Table 8: Summary of architectural parameters and cumulative synchronization data costs per team.

| Team | SL Baseline | Santhi | Elbflorenz | Camma |
|------------------------|----------------------------------|--------------------------------|---------------------------------|------------------------------|
| Parameters | 89,351,470 | 88,651,014 | 87,213,038 | 24,086,014 |
| Data Type | float32 (4 bytes/param) | float32 (4 bytes/param) | float32 (4 bytes/param) | float32 (4 bytes/param) |
| Model size | 357,405,880 B (340.85 MB) | 354,604,056 B (338.18 MB) | 348,852,152 B (332.69 MB) | 96,344,056 B (91.88 MB) |
| Clients | 3 | 3 | 3 | 3 |
| Sync Events | 100 | 20 | 50 | 10 |
| Total Costs | 142,962,352,000 B (133.14 GB) | 42,552,486,720 B (39.63 GB) | 104,655,645,600 B (97.47 GB) | 5,780,643,360 B (5.38 GB) |

4.1. The Role of Temporal Modeling

A key finding of this challenge is that temporal modeling strategy is the dominant performance factor, outweighing the choice of aggregation scheme or communication frequency. Frame-level approaches, whether operating through majority voting (Team Elbflorenz) or embedding-based prototype comparison (Team Camma), are inherently limited by the high intra-video visual variance present in laparoscopic recordings. Differences in laparoscopic hardware, lighting conditions, and patient anatomy render individual frames unreliable predictors of patient-level inflammation grade. The metric learning approach of Team Camma illustrates this most clearly: while it achieved competitive performance at centers whose visual characteristics were represented in training, it failed to map embeddings of the unseen center to established training prototypes, revealing the brittleness of a feature space built on individual frames.

Video-level temporal models, by contrast, capture the progression of visual features across the surgical sequence, providing contextual information no single frame can supply. The ViViT-based submission of Team Santhi, processing 32 frames jointly, consistently achieved the strongest generalization to the unseen center in Task 1, outperforming both frame-level approaches despite using fewer communication resources. This finding is consistent with prior work on decentralized surgical video analysis using the same dataset [22], in which temporal architectures similarly outperformed frame-level methods across patient-level prediction tasks.

With respect to the generalization vs. adaptation trade-off, temporal modeling also offered a partial advantage in Task 2: Team Santhi’s frozen ViViT backbone preserved global spatiotemporal representations during local fine-tuning, limiting the degree to which center-specific updates could corrupt the globally learned feature space. This suggests that architecture choice is not only a generalization strategy but also a safeguard against the instability of local adaptation. This point is revisited in Section 4.4.

4.2. Dataset Scale and Decentralization as Compounding Factors

The generally low absolute scores across all submissions raise an important question: do these results reflect fundamental limitations of FL, or primarily the difficulty of the task itself? The centralized baseline provides a direct answer. Even when pooling all multi-institutional data onto a single server, thereby removing all federated constraints, the centralized model achieved only 26.31% F1-score on the unseen center. This establishes that the underlying task of patient-level appendicitis grading from surgical video is intrinsically

difficult, regardless of the learning paradigm employed, due to the high visual variance across centers and the inherent ambiguity of fine-grained clinical grading.

Decentralization acts as an additional, separable bottleneck. The Swarm Learning baseline, which retains the same architecture as the centralized model but distributes training across centers, achieved 19.00% F1 in Task 1. This measurable degradation is attributable specifically to decentralized optimization across non-IID data nodes, rather than to any architectural deficiency. This gap quantifies what may be termed a decentralization penalty: the cost in predictive performance of preserving data privacy through distributed training. Together, the two baselines confirm that observed performance reflects a compounding of two distinct factors, and that algorithmic advances in FL aggregation must overcome both.

An additional consideration is the scale of the dataset. The challenge utilized 153 training videos, which constitute a preliminary subset of the 330-video Appendix300 dataset [21], distributed across four centers. At this data regime, FL fragments an already limited training pool, leaving individual nodes with insufficient samples to learn robust local representations. Prior work using the full dataset [22] demonstrated improved performance under decentralized training, suggesting that the current performance ceiling is partly a function of data scarcity rather than an inherent ceiling of the FL paradigm. Scaling the dataset, in terms of both total videos and number of contributing centers, is therefore a necessary condition for a more definitive evaluation of FL on surgical video.

4.3. Data Heterogeneity and the Limits of Local Adaptation

The challenge results highlight that non-IID data remains the central unsolved problem in federated surgical video analysis. Distribution shift across centers originates from two compounding sources: hardware-induced feature skew, including differences in laparoscopic systems, resolution, lighting, and cropping, and patient population heterogeneity, including differences in age distribution, disease severity prevalence, and surgical practice between academic and community centers. Current aggregation strategies, including FedAvg and FedSAM, partially mitigate but do not resolve these shifts.

These effects are further amplified by inter-center data quantity skew. Center 3 contributed 80 of the 153 training videos, causing global models to disproportionately reflect Center 3’s data distribution. The bootstrapped rank stability analysis illustrates the consequence: Task 1 rankings were stable, confirming that temporally-informed models were statistically distinguishable; Task 2 rankings showed pronounced instability, with no submission retaining its rank on the EC metric in more than 50% of bootstrap replicates. Local fine-tuning at smaller centers triggered reversion to trivial classifiers, predominantly predicting a single class as a consequence of catastrophic forgetting on heavily skewed local data, inflating nominal F1-scores without reflecting genuine adaptation. As discussed in Section 2.4, the EC metric was more robust to this artifact and should be considered the primary indicator of adaptation quality in imbalanced ordinal settings.

4.4. Toward Personalized Federated Learning

The results of both tasks point toward the same conclusion: a single globally aggregated model is a compromise that satisfies no center optimally. However, naive local fine-tuning, as evaluated in Task 2, does not resolve this, as unconstrained adaptation on skewed local data leads to catastrophic forgetting rather than genuine personalization. The path forward lies in structured personalized FL: approaches that separate a shared global representation from center-specific adaptation components, and train both with objectives that explicitly account for local data imbalance.

For Task 1 generalization, the FedSurg results support the use of a frozen pretrained temporal backbone as the globally federated component. By fixing backbone weights across federation rounds, center-specific visual variance cannot propagate into the shared representation, preserving its generalizability to unseen centers. Only lightweight task-specific heads need to be aggregated globally, substantially reducing both communication cost and the risk of conflicting updates between heterogeneous nodes.

For Task 2 adaptation, parameter-efficient fine-tuning (PEFT) methods offer a principled alternative to full local fine-tuning. Methods such as LoRA or adapter layers constrain the parameter space available for local updates, limiting the degree to which a small, imbalanced local dataset can destabilize the global representation, while still enabling meaningful center-specific adjustment. This approach is particularly relevant given the data regime of this challenge, where local node datasets ranged from 33 to 80 videos.

Looking further ahead, surgical video foundation models represent a promising direction for initializing the shared backbone [36, 37]. However, currently available surgical foundation models are trained on limited procedure-specific data, and general-purpose video foundation models produce feature spaces too broad for the fine-grained visual distinctions required in intraoperative grading tasks. Recent work combining FL with endoscopic foundation model pretraining [18] suggests a more principled path: federating the pretraining process itself to build privacy-preserving, domain-specific representations from the outset. The integration of such approaches with PEFT-based local adaptation remains a hypothesis for future evaluation rather than a validated recommendation.

The exploratory PEFT baselines included in this work provide initial empirical grounding for these recommendations. The EndoViT+LoRA variant, which applies LoRA to a frozen frame-level backbone, collapsed to majority-class prediction (Task 1 F1: 9.24%), confirming that parameter-efficient adaptation cannot compensate for the absence of temporal modeling in this data regime. The ViViT+LoRA variant, applying LoRA to a frozen temporal backbone, achieved 15.93% F1 on Task 1 and 29.57% F1 at Center 3 in Task 2, approaching the centralized baseline (32.67%) at the largest local node. Performance at smaller centers remained limited (Center 1: 12.22%, Center 2: 22.62%). This is consistent with the quantity-skew hypothesis: PEFT-based local adaptation is most effective where sufficient local samples are available to support stable fine-tuning.

4.5. Implications for Task Design

Beyond algorithmic choices, the FedSurg results suggest that the design of the clinical prediction task itself should inform the choice of FL strategy. This dimension has received limited attention in the literature. The consequences of prediction errors differ fundamentally between tasks, and these differences have direct implications for how generalization and adaptation should be balanced.

Consider two contrasting task types. In high-sensitivity settings, for example the detection of malignant lesions in colonoscopy where false negatives carry direct patient harm, global generalization to unseen centers is critical. FL strategies that prioritize robustness across non-IID distributions, such as flat-minima optimization approaches like FedSAM, are preferable over those that optimize local performance at the cost of cross-center generalizability. The fine-grained 6-class inflammation grading evaluated in this challenge approaches the opposite end of the spectrum: overcalling severity could influence clinical decision-making, placing greater weight on specificity. Here, the instability of local adaptation observed in Task 2 is particularly concerning. Classifier collapse, the reversion to a trivial classifier predominantly predicting a single class as a consequence

of catastrophic forgetting during fine-tuning on imbalanced local data, is not only a performance failure but a risk in high-specificity grading contexts.

These observations lead to a practical hypothesis for future work: FL strategy selection should be guided not only by dataset characteristics, but by an explicit analysis of the clinical error cost structure of the target task. High-sensitivity tasks call for globally robust aggregation; high-specificity tasks require adaptation strategies that prevent classifier collapse, such as the PEFT-based approaches discussed in Section 4.4. Systematic evaluation of this hypothesis across diverse surgical AI tasks remains an important open problem.

4.6. Limitations and Future Directions

Several limitations of this challenge should be acknowledged. Despite 24 registered teams, only three complete submissions were received, reflecting both the niche character of FL within surgical AI and the high technical barriers to participation. The dataset, as a preliminary subset of Appendix300 [21], was insufficient in scale for robust federated training, and the simulated FL setup, where all data resided centrally during evaluation, does not capture the full complexity of real-world distributed deployments, including network latency, node availability, and hardware heterogeneity. Future work should prioritize scaling the dataset across a broader network of institutions and transitioning from simulated to genuine multi-institutional FL. On the algorithmic side, imbalance-aware objectives, such as federated focal loss or client-weighted aggregation, and personalized aggregation methods that account for quantity skew are necessary next steps. Self-supervised pretraining on large-scale surgical video collections, ideally in a federated manner [18], offers a promising route toward more transferable representations without compromising data privacy.

5. Conclusion

The FedSurg Challenge establishes the first benchmark for FL in surgical video classification, evaluated here as a proof-of-concept using a multi-center dataset of laparoscopic appendectomies. The results reveal that temporal modeling is the dominant architectural factor for cross-center generalization, while decentralized training introduces a measurable performance penalty on top of the intrinsic difficulty of the task. Local fine-tuning without imbalance-aware objectives leads to classifier collapse rather than genuine personalization, underscoring the need for structured personalized FL with parameter-efficient adaptation. By characterizing these failure modes through rigorous statistical analysis, this work provides a methodological reference point for the design of robust, privacy-preserving AI systems for surgical video analysis and motivates future benchmarking on tasks with broader clinical scope.

Acknowledgments

This work was co-funded by the European Union through NEARDATA under grant agreement ID 101092644, the German Research Foundation (DFG, Deutsche Forschungsgemeinschaft) as part of Germany’s Excellence Strategy – EXC 2050/1 – Project ID 390696704 – Cluster of Excellence “Centre for Tactile Internet with Human-in-the-Loop” (CeTI) of Dresden University of Technology, and the Federal Ministry of Education and Research of Germany in the program of “Souverän. Digital. Vernetzt.”, a joint project 6G-life with the project identification number 16KISK001K.

Furthermore, FRK receives support from the German Cancer Research Center (CoBot 2.0), the Joachim Herz Foundation (Add-On Fellowship for Interdisciplinary Life Science), the Central Indiana Corporate Partnership AnalytiXIN Initiative, the Evan and Sue Ann Werling Pancreatic Cancer Research Fund, and the Indiana Clinical and Translational Sciences Institute (EPAR4157) funded, in part, by Grant Number UM1TR004402 from the National Institutes of Health, National Center for Advancing Translational Sciences, Clinical and Translational Sciences Award. The content is solely the responsibility of the authors and does not necessarily represent the official views of the National Institutes of Health.

Team CAMMA (NP, JA) was supported by French State Funds managed by the Agence Nationale de la Recherche (ANR) under Grants ANR-22-FAI1-0001 (Project DAIOR) and ANR-10-IAHU-02 (IHU Strasbourg).

Conflict of Interest

JNK declares consulting services for Biopimus, France; Panakeia, UK; AstraZeneca, UK; and MultiplexDx, Slovakia. Furthermore, he holds shares in StratifAI, Germany, Synagen, Germany, Ignition Lab, Germany; has received an institutional research grant by GSK; and has received honoraria by AstraZeneca, Bayer, Daiichi Sankyo, Eisai, Janssen, Merck, MSD, BMS, Roche, Pfizer, and Fresenius.

FRK declares advisory roles for Radical Healthcare, USA; and the Surgical Data Science Collective, USA, and has received research funding from Novartis.

SS received speaker's fees from Stryker Corporation.

AR, NP, SS, DS, and SBa serve as an Associate Editor for the Medical Image Analysis journal.

NP is co-founder and owns shares in Scialytics SAS.

Declaration of generative AI and AI-assisted technologies in the writing process.

During the preparation of this work, the author(s) used ChatGPT, Gemini 2.5 Pro, Claude Code, and DeepL Write in order to improve the readability and language of the manuscript. After using these tools/services, the author(s) reviewed and edited the content as needed and take full responsibility for the content of the published article.

Appendix A. Dataset and Annotation Protocol

The challenge dataset is a preliminary subset of the publicly available Appendix300 dataset [21]. A CSV file detailing the samples used in the challenge is available here ², along with two videos that were excluded from the final dataset but used in the challenge for reproducibility. The dataset is available for non-commercial use under a CC BY license and requires citation of the Appendix300 publication. The annotation protocol is available in [21]. Usage of the data for individual publications was prohibited before the release of this study and the Appendix300 dataset.

²Available at <https://nextcloud.tso.ukdd.de/s/XppWkRnWpLGwj5F> Password for Review: FedSurg24_data!

Appendix B. Challenge Rules

During registration, participants signed the EndoVis rules document³.

Appendix C. Challenge Organization

This work was jointly organized by four parties. Fiona R. Kolbinger, from the Department of Visceral, Thoracic and Vascular Surgery, Faculty of Medicine and University Hospital Carl Gustav Carus of the TUD Dresden University of Technology and the Weldon School of Biomedical Engineering, Purdue University coordinated the challenge data collection from four hospitals in Germany. Oliver L. Saldanha and Jakob N. Kather, also from the Else Kröner Fresenius Center for Digital Health, supported the data aggregation from the technical point of view and obtained the source data from these centers. Max Kirchner, Alexander C. Jenke, Sebastian Bodenstedt, and Stefanie Speidel, from the Department of Translational Surgical Oncology (TSO) of the National Center for Tumor Diseases (NCT) Dresden, supported data aggregation and carried out the challenge organization and the technical implementation, including preprocessing, data provision, participant registration and administration, submission handling, evaluation, and results presentation. The NearData Horizon Europe program provided €500 in prize money, equally distributed across both tasks. If a single team achieved the top score in both tasks, they were eligible to receive both awards.

Appendix D. Submission Instructions

The submission process was described in detail on the official challenge website⁴. To support development, an example setup based on the FL Flower framework [34] was provided through a GitLab repository⁵. The evaluation framework was made transparent through another repository⁶, which included the source code for metric computation as well as the ranking scripts (bootstrapping, statistical testing, and related plots).

Participants submitted their solutions as Docker containers via the challenge website. Docker Compose scripts with additional code were also accepted, provided they encapsulated the complete FL algorithm for both training and inference. Submissions had to run fully automatically without user interaction. Participants received email notifications about submission status and were allowed unlimited resubmissions until the final deadline. While the organizers do not distribute Docker images, teams were encouraged to release their code publicly.

Appendix E. Challenge design document

See Supplementary file S1.

³Available at <https://tinyurl.com/nhb5z6a3>

⁴Available at <https://www.synapse.org/Synapse:syn53137385/wiki/625370>

⁵Available at https://gitlab.com/nct_tso_public/challenges/miccai2024/FedSurg24

⁶Available at https://gitlab.com/nct_tso_public/challenges/miccai2024/snippet

Appendix F. Ethics approval

This study was prospectively reviewed and approved by the Institutional Review Board of the TUD Dresden University of Technology, Germany (approval number: BO-EK-332072022, approval date: August 4, 2022). The corresponding study was prospectively registered at the German Registry of Clinical Trials (DRKS, URL, registration ID DRKS00030874).

Appendix G. Additional Bootstrapping and Wilcoxon Signed-Rank Test Results

Table G.9: Bootstrap rank frequency, win probability, and Wilcoxon signed-rank p -values for both tasks (F1-score).

| Task | Center | Team | Rank Freq. | | | Win Prob. | | | Wilcox p | | |
|------|--------|------|---------------|---------------|---------------|-----------|--------|--------|------------|-------------------------|-------------------------|
| | | | 1 | 2 | 3 | Cam | Elb | San | Cam | Elb | San |
| 1 | 4 | Cam | 0.0000 | 0.2491 | 0.7509 | NaN | 0.2481 | 0.0000 | NaN | 0.0000 | 0.0000 |
| 1 | 4 | Elb | 0.0077 | 0.7442 | 0.2481 | 0.7509 | NaN | 0.0077 | 0.0000 | NaN | 0.0000 |
| 1 | 4 | San | 0.9923 | 0.0077 | 0.0000 | 1.0000 | 0.9923 | NaN | 0.0000 | 0.0000 | NaN |
| 2 | Avg | Cam | 0.7192 | 0.1994 | 0.0814 | NaN | 0.8501 | 0.7876 | NaN | 0.0000 | 0.0000 |
| 2 | Avg | Elb | 0.1023 | 0.3503 | 0.5474 | 0.1499 | NaN | 0.4050 | 0.0000 | NaN | 5.04×10^{-106} |
| 2 | Avg | San | 0.1786 | 0.4502 | 0.3712 | 0.2123 | 0.5950 | NaN | 0.0000 | 5.04×10^{-106} | NaN |

Table G.10: Bootstrap rank frequency, win probability, and Wilcoxon signed-rank p -values for both tasks (EC).

| Task | Center | Team | Rank Freq. | | | Win Prob. | | | Wilcox p | | |
|------|--------|------|---------------|---------------|---------------|-----------|--------|--------|-------------------------|-------------------------|-------------------------|
| | | | 1 | 2 | 3 | Cam | Elb | San | Cam | Elb | San |
| 1 | 4 | Cam | 0.0000 | 0.0000 | 1.0000 | NaN | 0.0000 | 0.0000 | NaN | 0.0000 | 0.0000 |
| 1 | 4 | Elb | 0.0027 | 0.9973 | 0.0000 | 1.0000 | NaN | 0.0021 | 0.0000 | NaN | 0.0000 |
| 1 | 4 | San | 0.9979 | 0.0021 | 0.0000 | 1.0000 | 0.9973 | NaN | 0.0000 | 0.0000 | NaN |
| 2 | Avg | Cam | 0.2781 | 0.2955 | 0.4264 | NaN | 0.4661 | 0.3791 | NaN | 3.13×10^{-13} | 1.15×10^{-177} |
| 2 | Avg | Elb | 0.2855 | 0.3646 | 0.3499 | 0.5307 | NaN | 0.3991 | 3.13×10^{-13} | NaN | 1.17×10^{-128} |
| 2 | Avg | San | 0.4412 | 0.3394 | 0.2194 | 0.6176 | 0.5983 | NaN | 1.15×10^{-177} | 1.17×10^{-128} | NaN |

Appendix H. Further Analysis Results with Baselines

Table H.11: Comprehensive ranking summary for Task 1, Task 2, and overall performance including contextual baselines. Lower rank indicates better performance.

| Team | Task 1 | | | Task 2 | | | Overall Avg | Final Rank |
|------------|--------|----|-----|--------|----|-----|-------------|------------|
| | EC | F1 | Avg | EC | F1 | Avg | | |
| Camma | 5 | 5 | 5 | 5 | 2 | 3 | 4.00 | 3 |
| Elbflorenz | 4 | 4 | 4 | 4 | 5 | 4 | 4.00 | 3 |
| Santhi | 2 | 2 | 2 | 3 | 4 | 3 | 2.50 | 2 |
| Cen | 1 | 1 | 1 | 1 | 1 | 1 | 1.00 | 1 |
| SWARM | 3 | 3 | 3 | 2 | 3 | 2 | 2.50 | 2 |

Appendix H.0.1. Detailed Bootstrap Analysis Tables

Task 1: Generalization (F1-score). Tables H.12–H.14 report rank frequency, pairwise win probabilities, and Wilcoxon p -values for Task 1 F1-score. Rankings are stable: the centralized baseline holds rank 1 in 67.0% of bootstrap iterations and all pairwise comparisons are statistically significant ($p < 0.001$).

Table H.12: Task 1 F1-score: Rank frequency distribution.

| Team | Rank 1 | Rank 2 | Rank 3 | Rank 4 | Rank 5 |
|------------|--------|--------|--------|--------|--------|
| Camma | 0.0000 | 0.0000 | 0.0007 | 0.2486 | 0.7507 |
| Elbflorenz | 0.0002 | 0.0022 | 0.0111 | 0.7385 | 0.2480 |
| Santhi | 0.2961 | 0.4736 | 0.2233 | 0.0070 | 0.0000 |
| Cen | 0.6700 | 0.2917 | 0.0377 | 0.0005 | 0.0001 |
| SWARM | 0.0350 | 0.2319 | 0.7265 | 0.0065 | 0.0001 |

Table H.13: Task 1 F1-score: Pairwise win probabilities $P(\text{team}_i > \text{team}_j)$.

| Team | Camma | Elbflorenz | Santhi | Cen | SWARM |
|------------|--------|------------|--------|--------|--------|
| Camma | — | 0.2481 | 0.0000 | 0.0001 | 0.0007 |
| Elbflorenz | 0.7509 | — | 0.0077 | 0.0011 | 0.0074 |
| Santhi | 1.0000 | 0.9923 | — | 0.3024 | 0.7637 |
| Cen | 0.9999 | 0.9989 | 0.6974 | — | 0.9330 |
| SWARM | 0.9992 | 0.9926 | 0.2361 | 0.0654 | — |

Table H.14: Task 1 F1-score: Wilcoxon p-values. All comparisons $p < 0.001$.

| Team | Camma | Elbflorenz | Santhi | Cen | SWARM |
|------------|-------|------------|--------|-------|-------|
| Camma | — | 0.000 | 0.000 | 0.000 | 0.000 |
| Elbflorenz | 0.000 | — | 0.000 | 0.000 | 0.000 |
| Santhi | 0.000 | 0.000 | — | 0.000 | 0.000 |
| Cen | 0.000 | 0.000 | 0.000 | — | 0.000 |
| SWARM | 0.000 | 0.000 | 0.000 | 0.000 | — |

Table H.15: Task 1 EC: Rank frequency distribution.

| Team | Rank 1 | Rank 2 | Rank 3 | Rank 4 | Rank 5 |
|------------|--------|--------|--------|--------|--------|
| Camma | 0.0000 | 0.0000 | 0.0000 | 0.0000 | 1.0000 |
| Elbflorenz | 0.0000 | 0.0005 | 0.0035 | 0.9960 | 0.0000 |
| Santhi | 0.2576 | 0.3401 | 0.4003 | 0.0020 | 0.0000 |
| Cen | 0.7384 | 0.2480 | 0.0136 | 0.0000 | 0.0000 |
| SWARM | 0.1021 | 0.3715 | 0.5254 | 0.0010 | 0.0000 |

Table H.16: Task 1 EC: Pairwise win probabilities.

| Team | Camma | Elbflorenz | Santhi | Cen | SWARM |
|------------|--------|------------|--------|--------|--------|
| Camma | — | 0.0000 | 0.0000 | 0.0000 | 0.0000 |
| Elbflorenz | 1.0000 | — | 0.0021 | 0.0001 | 0.0013 |
| Santhi | 1.0000 | 0.9973 | — | 0.2048 | 0.5382 |
| Cen | 1.0000 | 0.9999 | 0.7355 | — | 0.8858 |
| SWARM | 1.0000 | 0.9983 | 0.4091 | 0.0703 | — |

Table H.17: Task 1 EC: Wilcoxon p-values. All highly significant ($p < 0.001$).

| Team | Camma | Elbflorenz | Santhi | Cen | SWARM |
|------------|-------|------------|------------------------|-------|------------------------|
| Camma | — | 0.000 | 0.000 | 0.000 | 0.000 |
| Elbflorenz | 0.000 | — | 0.000 | 0.000 | 0.000 |
| Santhi | 0.000 | 0.000 | — | 0.000 | 2.89×10^{-65} |
| Cen | 0.000 | 0.000 | 0.000 | — | 0.000 |
| SWARM | 0.000 | 0.000 | 2.89×10^{-65} | 0.000 | — |

Task 1: Generalization (Expected Cost). Tables H.15–H.17 report the equivalent analysis for the EC metric. Rankings are similarly stable, with Camma retaining the last rank in 100% of iterations and all pairwise differences statistically significant.

Task 2: Adaptation (F1-score). Tables H.18–H.20 show markedly higher rank volatility compared to Task 1. No team retains a single rank in more than 66.4% of iterations, and the pairwise win probabilities between Camma, Santhi, and SL indicate substantial overlap, reflecting the instability of local adaptation across centers.

Task 2: Adaptation (Expected Cost). Tables H.21–H.23 report Task 2 EC bootstrap results, where rank instability is most pronounced. Rank frequencies are close to uniform for most teams, confirming that EC-based adaptation rankings are not reliably reproducible under resampling and should be interpreted with caution.

Table H.18: Task 2 F1-score: Rank frequency distribution.

| Team | Rank 1 | Rank 2 | Rank 3 | Rank 4 | Rank 5 |
|------------|--------|--------|--------|--------|--------|
| Camma | 0.1794 | 0.3490 | 0.2499 | 0.1517 | 0.0700 |
| Elbflorenz | 0.0078 | 0.0517 | 0.1407 | 0.3063 | 0.4935 |
| Santhi | 0.0153 | 0.0992 | 0.2188 | 0.3254 | 0.3413 |
| Cen | 0.6641 | 0.1999 | 0.0866 | 0.0367 | 0.0127 |
| SWARM | 0.1335 | 0.3001 | 0.3041 | 0.1798 | 0.0825 |

Table H.19: Task 2 F1-score: Pairwise win probabilities.

| Team | Camma | Elbflorenz | Santhi | Cen | SWARM |
|------------|--------|------------|--------|--------|--------|
| Camma | — | 0.8507 | 0.7786 | 0.2326 | 0.5540 |
| Elbflorenz | 0.1493 | — | 0.4091 | 0.0408 | 0.1748 |
| Santhi | 0.2212 | 0.5909 | — | 0.0648 | 0.2447 |
| Cen | 0.7674 | 0.9592 | 0.9352 | — | 0.8042 |
| SWARM | 0.4460 | 0.8252 | 0.7553 | 0.1958 | — |

Table H.20: Task 2 F1-score: Wilcoxon p-values.

| Team | Camma | Elbflorenz | Santhi | Cen | SWARM |
|------------|------------------------|-------------------------|--------|-------|------------------------|
| Camma | — | 0.000 | 0.000 | 0.000 | 9.54×10^{-35} |
| Elbflorenz | 0.000 | — | 0.000 | 0.000 | 0.000 |
| Santhi | 0.000 | 1.49×10^{-101} | — | 0.000 | 0.000 |
| Cen | 0.000 | 0.000 | 0.000 | — | 0.000 |
| SWARM | 9.54×10^{-35} | 0.000 | 0.000 | 0.000 | — |

Table H.21: Task 2 EC: Rank frequency distribution.

| Team | Rank 1 | Rank 2 | Rank 3 | Rank 4 | Rank 5 |
|------------|--------|--------|--------|--------|--------|
| Camma | 0.1367 | 0.1533 | 0.1737 | 0.2169 | 0.3194 |
| Elbflorenz | 0.1262 | 0.1773 | 0.2202 | 0.2377 | 0.2386 |
| Santhi | 0.2035 | 0.2317 | 0.2299 | 0.1956 | 0.1393 |
| Cen | 0.3043 | 0.2228 | 0.1840 | 0.1628 | 0.1261 |
| SWARM | 0.2323 | 0.2154 | 0.1933 | 0.1849 | 0.1741 |

Table H.22: Task 2 EC: Pairwise win probabilities.

| Team | Camma | Elbflorenz | Santhi | Cen | SWARM |
|------------|--------|------------|--------|--------|--------|
| Camma | — | 0.4637 | 0.3791 | 0.3333 | 0.3872 |
| Elbflorenz | 0.5336 | — | 0.4015 | 0.3571 | 0.4156 |
| Santhi | 0.6166 | 0.5954 | — | 0.4415 | 0.5026 |
| Cen | 0.6665 | 0.6422 | 0.5578 | — | 0.5477 |
| SWARM | 0.6123 | 0.5839 | 0.4971 | 0.4517 | — |

Table H.23: Task 2 EC: Wilcoxon p-values. Note: Santhi vs. SWARM $p = 0.746$ (not significant).

| Team | Camma | Elbflorenz | Santhi | Cen | SWARM |
|------------|-------------------------|------------------------|-------------------------|------------------------|-------------------------|
| Camma | — | 1.30×10^{-21} | 2.72×10^{-189} | 0.000 | 1.21×10^{-171} |
| Elbflorenz | 1.30×10^{-21} | — | 3.81×10^{-72} | 0.000 | 4.71×10^{-98} |
| Santhi | 2.72×10^{-189} | 3.81×10^{-72} | — | 0.000 | 0.746 |
| Cen | 0.000 | 0.000 | 0.000 | — | 2.86×10^{-38} |
| SWARM | 1.21×10^{-171} | 4.71×10^{-98} | 0.746 | 2.86×10^{-38} | — |

Appendix I. Credit Authorship Contribution Statement

Max Kirchner: Conceptualization, Challenge Organization, Methodology, Software, Validation, Formal Analysis, Investigation, Data Curation, Writing - Original Draft, Writing - Review and Editing, Visualization, Project Administration **Hanna Hoffmann:** Conceptualization, Software, Writing - Review and Editing **Alexander C. Jenke:** Challenge Organization, Software, Writing - Review and Editing **Oliver L. Saldanha:** Conceptualization, Challenge Organization, Software, Investigation, Data Curation, Writing - Review and Editing **Kevin Pfeiffer:** Software, Data Curation, Writing - Review and Editing **Kanjo Weam:** Data Curation, Writing - Review and Editing **Julia Alekseenko:** Methodology, Software, Investigation, Visualization, Writing - Review and Editing **Claas de Boer:** Methodology, Software, Investigation, Writing - Review and Editing **Santhi Raj Kolamuri:** Methodology, Software, Investigation, Writing - Review and Editing **Lorenzo Mazza:** Methodology, Software, Investigation, Writing - Review and Editing **Nicolas Padoy:** Challenge Team Supervision, Writing - Review and Editing **Sophia Bano:** Challenge Organization, Supervision, Writing - Review and Editing **Annika Reinke:** Conceptualization, Challenge Organization, Supervision, Writing - Review and Editing **Lena Maier-Hein:** Challenge Organization, Supervision, Writing - Review and Editing **Danail Stoyanov:** Challenge Organization, Supervision, Writing - Review and Editing **Jakob N. Kather:** Conceptualization, Challenge Organization, Writing - Review and Editing, Supervision, Project administration, Funding Acquisition **Fiona R. Kolbinger:** Conceptualization, Challenge Organization, Investigation, Data Curation, Writing - Review and Editing, Supervision, Project Administration, Funding Acquisition **Sebastian Bodenstedt:** Conceptualization, Challenge Organization, Software, Investigation, Data Curation, Writing - Review and Editing, Supervision, Project Administration, Funding Acquisition, Challenge Team Supervision **Stefanie Speidel:** Conceptualization, Challenge Organization, Writing - Review and Editing, Supervision, Project Administration, Funding Acquisition, Challenge Team Supervision

References

- [1] L. Maier-Hein, S. Vedula, S. Speidel, N. Navab, R. Kikinis, A. Park, M. Eisenmann, H. Feussner, G. Forestier, S. Giannarou, M. Hashizume, D. Katić, H. Kenngott, M. Kranzfelder, A. Malpani, K. März, T. Neumuth, N. Padoy, C. Pugh, P. Jannin, Surgical data science for next-generation interventions, *Nature Biomedical Engineering* 1 (Sep. 2017). doi:10.1038/s41551-017-0132-7.
- [2] J. M. Brandenburg, A. C. Jenke, A. Stern, M. T. J. Daum, A. Schulze, R. Younis, P. Petrynowski, T. Davitashvili, V. Vanat, N. Bhasker, S. Schneider, L. Mündermann, A. Reinke, F. R. Kolbinger, V. Jörns, F. Fritz-Kebede, M. Dugas, L. Maier-Hein, R. Klotz, M. Distler, J. Weitz, B. P. Müller-Stich, S. Speidel, S. Bodenstedt, M. Wagner, Active learning for extracting surgomic features in robot-assisted minimally invasive esophagectomy: a prospective annotation study, *Surgical Endoscopy* 37 (11) (2023) 8577–8593. doi:10.1007/s00464-023-10447-6.
URL <https://doi.org/10.1007/s00464-023-10447-6>
- [3] L. Maier-Hein, M. Eisenmann, D. Sarikaya, K. März, T. Collins, A. Malpani, J. Fallert, H. Feussner, S. Giannarou, P. Mascagni, H. Nakawala, A. Park, C. Pugh, D. Stoyanov, S. S. Vedula, K. Cleary, G. Fichtinger, G. Forestier, B. Gibaud, T. Grantcharov, M. Hashizume, D. Heckmann-Nötzel, H. G. Kenngott, R. Kikinis, L. Mündermann, N. Navab, S. Onogur, T. Roß, R. Sznitman, R. H. Taylor, M. D. Tizabi, M. Wagner, G. D. Hager, T. Neumuth, N. Padoy, J. Collins, I. Gockel, J. Goedeke, D. A. Hashimoto, L. Joyeux, K. Lam, D. R. Leff, A. Madani, H. J. Marcus, O. Meireles, A. Seitel, D. Teber, F. Ückert, B. P. Müller-Stich, P. Jannin, S. Speidel, Surgical data science – from concepts toward clinical translation, *Medical Image Analysis* 76 (2022) 102306. doi:10.1016/j.media.2021.102306.
URL <https://www.sciencedirect.com/science/article/pii/S1361841521003510>
- [4] M. Carstens, S. Vasisht, Z. Zhang, I. Barbur, A. Reinke, L. Maier-Hein, D. A. Hashimoto, F. R. Kolbinger, Artificial intelligence for surgical scene understanding: A systematic review and reporting quality meta-analysis, ISSN: 3067-2007 Pages: 2025.07.12.25330122 (2025). doi:10.1101/2025.07.12.25330122.
URL <https://www.medrxiv.org/content/10.1101/2025.07.12.25330122v1>
- [5] K. Kirtac, N. Aydin, J. Lavanchy, G. Beldi, M. Smit, M. Woods, F. Aspart, Surgical Phase Recognition: From Public Datasets to Real-World Data, *Applied Sciences* 12 (2022) 8746. doi:10.3390/app12178746.
- [6] J. L. Lavanchy, S. Ramesh, D. Dall’Alba, C. Gonzalez, P. Fiorini, B. Muller-Stich, P. C. Nett, J. Marescaux, D. Mutter, N. Padoy, Challenges in Multi-centric Generalization: Phase and Step Recognition in Roux-en-Y Gastric Bypass Surgery, arXiv:2312.11250 [cs] (Dec. 2023). doi:10.48550/arXiv.2312.11250.
URL <http://arxiv.org/abs/2312.11250>
- [7] O. f. C. Rights (OCR), Health information privacy, last Modified: 2025-06-27T11:38:47-0400 (2021).
URL <https://www.hhs.gov/hipaa/index.html>

- [8] General data protection regulation (GDPR) – legal text (2016).
URL <https://gdpr-info.eu/>
- [9] B. McMahan, E. Moore, D. Ramage, S. Hampson, B. A. y. Arcas, Communication-Efficient Learning of Deep Networks from Decentralized Data, in: Proceedings of the 20th International Conference on Artificial Intelligence and Statistics, PMLR, 2017, pp. 1273–1282, iSSN: 2640-3498.
URL <https://proceedings.mlr.press/v54/mcmahan17a.html>
- [10] D. Yin, Y. Chen, R. Kannan, P. Bartlett, Byzantine-Robust Distributed Learning: Towards Optimal Statistical Rates, in: Proceedings of the 35th International Conference on Machine Learning, PMLR, 2018, pp. 5650–5659, iSSN: 2640-3498.
URL <https://proceedings.mlr.press/v80/yin18a.html>
- [11] N. Rieke, J. Hancox, W. Li, F. Milletari, H. R. Roth, S. Albarqouni, S. Bakas, M. N. Galtier, B. A. Landman, K. Maier-Hein, S. Ourselin, M. Sheller, R. M. Summers, A. Trask, D. Xu, M. Baust, M. J. Cardoso, The future of digital health with federated learning, *npj Digital Medicine* 3 (1) (2020) 119, publisher: Nature Publishing Group. doi:10.1038/s41746-020-00323-1.
URL <https://www.nature.com/articles/s41746-020-00323-1>
- [12] T. Li, A. K. Sahu, A. Talwalkar, V. Smith, Federated Learning: Challenges, Methods, and Future Directions, *IEEE Signal Processing Magazine* 37 (3) (2020) 50–60. doi:10.1109/MSP.2020.2975749.
URL <https://ieeexplore.ieee.org/document/9084352>
- [13] P. Kairouz, H. B. McMahan, B. Avent, A. Bellet, M. Bennis, A. N. Bhagoji, K. Bonawitz, Z. Charles, G. Cormode, R. Cummings, R. G. L. D’Oliveira, H. Eichner, S. E. Rouayheb, D. Evans, J. Gardner, Z. Garrett, A. Gascón, B. Ghazi, P. B. Gibbons, M. Gruteser, Z. Harchaoui, C. He, L. He, Z. Huo, B. Hutchinson, J. Hsu, M. Jaggi, T. Javidi, G. Joshi, M. Khodak, J. Konečný, A. Korolova, F. Koushanfar, S. Koyejo, T. Lepoint, Y. Liu, P. Mittal, M. Mohri, R. Nock, A. Özgür, R. Pagh, M. Raykova, H. Qi, D. Ramage, R. Raskar, D. Song, W. Song, S. U. Stich, Z. Sun, A. T. Suresh, F. Tramèr, P. Vepakomma, J. Wang, L. Xiong, Z. Xu, Q. Yang, F. X. Yu, H. Yu, S. Zhao, Advances and open problems in federated learning (2021). arXiv:1912.04977[cs], doi:10.48550/arXiv.1912.04977.
URL <http://arxiv.org/abs/1912.04977>
- [14] A. Rauniar, D. H. Hagos, D. Jha, J. E. Håkegård, U. Bagci, D. B. Rawat, V. Vlassov, Federated learning for medical applications: A taxonomy, current trends, challenges, and future research directions (2023). arXiv:2208.03392[cs], doi:10.48550/arXiv.2208.03392.
URL <http://arxiv.org/abs/2208.03392>
- [15] A. Z. Tan, H. Yu, L. Cui, Q. Yang, Towards personalized federated learning, *IEEE Transactions on Neural Networks and Learning Systems* 34 (12) (2023) 9587–9603. doi:10.1109/TNNLS.2022.3160699.
- [16] T. Li, M. Sanjabi, A. Beirami, V. Smith, Fair resource allocation in federated learning (2020). arXiv:1905.10497[cs], doi:10.48550/arXiv.1905.10497.
URL <http://arxiv.org/abs/1905.10497>

- [17] H. Kassem, D. Alapatt, P. Mascagni, C. AI4SafeChole, A. Karargyris, N. Padoy, Federated cycling (FedCy): Semi-supervised federated learning of surgical phases, *IEEE Transactions on Medical Imaging* (2022) 1–1Conference Name: *IEEE Transactions on Medical Imaging*. doi:10.1109/TMI.2022.3222126.
- [18] M. Kirchner, A. C. Jenke, S. Bodenstedt, F. R. Kolbinger, O. L. Saldanha, J. N. Kather, M. Wagner, S. Speidel, Federated EndoViT: Pretraining Vision Transformers via Federated Learning on Endoscopic Image Collections, *arXivArXiv:2504.16612 [cs]* (May 2025). doi:10.48550/arXiv.2504.16612.
URL <http://arxiv.org/abs/2504.16612>
- [19] Y. Li, S. S. Kundu, M. Boels, T. Mahmoodi, S. Ourselin, T. Vercauteren, P. Dasgupta, J. Shapey, A. Granados, UltraFlwr – an efficient federated medical and surgical object detection framework (2025). *arXiv:2503.15161 [cs]*, doi:10.48550/arXiv.2503.15161.
URL <http://arxiv.org/abs/2503.15161>
- [20] S. Speidel, L. Maier-Hein, D. Stoyanov, S. Bodenstedt, A. Reinke, S. Bano, Endoscopic Vision Challenge – A MICCAI Challenge.
URL <https://opencas.dkfz.de/endovis/>
- [21] F. R. Kolbinger, M. Kirchner, K. Pfeiffer, S. Bodenstedt, A. C. Jenke, J. Barthel, M. R. Carstens, K. Dehlke, S. Dietz, S. Emmanouilidis, G. Fitze, L. Leitermann, S. T. Mees, S. Pistorius, C. Prudlo, A. Seiberth, J. Schultz, K. Thiel, D. Ziehn, S. Speidel, J. Weitz, J. N. Kather, M. Distler, O. L. Saldanha, Appendix300: A multi-institutional laparoscopic appendectomy video dataset for computational modeling tasks, *ISSN: 3067-2007 Pages: 2025.09.05.25335174*. doi:10.1101/2025.09.05.25335174.
URL <https://www.medrxiv.org/content/10.1101/2025.09.05.25335174v1>
- [22] O. L. Saldanha, K. Pfeiffer, S. Bodenstedt, M. Kirchner, A. C. Jenke, C. Barata, S. Barbosa, J. Barthel, M. Carstens, L. T. Castro, K. Dehlke, S. Dietz, S. Emmanouilidis, G. Fitze, M. Freitag, F. Holderried, W. Kanjo, L. Leitermann, S. T. Mees, A. S. Soares, M. Pascoal, S. Pistorius, C. Prudlo, J. Schultz, A. Seiberth, K. Thiel, X. Wu, D. Ziehn, S. Speidel, J. Weitz, M. Distler, J. N. Kather, F. R. Kolbinger, Decentralized, privacy-preserving surgical video analysis with swarm learning, in preparation.
- [23] L. Maier-Hein, A. Reinke, M. Kozubek, A. L. Martel, T. Arbel, M. Eisenmann, A. Hanbury, P. Jannin, H. Müller, S. Onogur, J. Saez-Rodriguez, B. van Ginneken, A. Kopp-Schneider, B. A. Landman, BIAS: Transparent reporting of biomedical image analysis challenges, *Medical Image Analysis* 66 (2020) 101796. doi:10.1016/j.media.2020.101796.
URL <https://www.sciencedirect.com/science/article/pii/S1361841520301602>
- [24] C. A. Gomes, T. A. Nunes, J. M. Fonseca Chebli, C. S. Junior, C. C. Gomes, Laparoscopy grading system of acute appendicitis: new insight for future trials, *Surgical Laparoscopy, Endoscopy & Percutaneous Techniques* 22 (5) (2012) 463–466. doi:10.1097/SLE.0b013e318262edf1.

- [25] S. Tomar, Converting video formats with ffmpeg, *Linux Journal* 2006 (146) (2006) 10.
- [26] L. R. Dice, Measures of the amount of ecologic association between species, *Ecology* 26 (3) (1945) 297–302, [_eprint: https://esajournals.onlinelibrary.wiley.com/doi/pdf/10.2307/1932409](https://esajournals.onlinelibrary.wiley.com/doi/pdf/10.2307/1932409). doi: 10.2307/1932409.
URL <https://onlinelibrary.wiley.com/doi/abs/10.2307/1932409>
- [27] L. Maier-Hein, A. Reinke, P. Godau, M. D. Tizabi, F. Buettner, E. Christodoulou, B. Glocker, F. Isensee, J. Kleesiek, M. Kozubek, M. Reyes, M. A. Riegler, M. Wiesenfath, A. E. Kavur, C. H. Sudre, M. Baumgartner, M. Eisenmann, D. Heckmann-Nötzl, T. Rädtsch, L. Acion, M. Antonelli, T. Arbel, S. Bakas, A. Benis, M. B. Blaschko, M. J. Cardoso, V. Cheplygina, B. A. Cimini, G. S. Collins, K. Farahani, L. Ferrer, A. Galdran, B. Van Ginneken, R. Haase, D. A. Hashimoto, M. M. Hoffman, M. Huisman, P. Jannin, C. E. Kahn, D. Kainmueller, B. Kainz, A. Karargyris, A. Karthikesalingam, F. Kofler, A. Kopp-Schneider, A. Kreshuk, T. Kurc, B. A. Landman, G. Litjens, A. Madani, K. Maier-Hein, A. L. Martel, P. Mattson, E. Meijering, B. Menze, K. G. M. Moons, H. Müller, B. Niyhoporuk, F. Nickel, J. Petersen, N. Rajpoot, N. Rieke, J. Saez-Rodriguez, C. I. Sánchez, S. Shetty, M. Van Smeden, R. M. Summers, A. A. Taha, A. Tiulpin, S. A. Tsaftaris, B. Van Calster, G. Varoquaux, P. F. Jäger, Metrics reloaded: recommendations for image analysis validation, *Nature Methods* 21 (2) (2024) 195–212. doi:10.1038/s41592-023-02151-z.
URL <https://www.nature.com/articles/s41592-023-02151-z>
- [28] T. Hastie, R. Tibshirani, J. H. Friedman, J. H. Friedman, *The elements of statistical learning: data mining, inference, and prediction*, Vol. 2, Springer, 2009.
- [29] C. Elkan, The foundations of cost-sensitive learning, in: *Proceedings of the 17th International Joint Conference on Artificial Intelligence (IJCAI)*, 2001, pp. 973–978.
- [30] B. Efron, Bootstrap methods: another look at the jackknife, in: *Breakthroughs in statistics: Methodology and distribution*, Springer, 1992, pp. 569–593.
- [31] L. Maier-Hein, M. Eisenmann, A. Reinke, S. Onogur, M. Stankovic, P. Scholz, T. Arbel, H. Bogunovic, A. P. Bradley, A. Carass, C. Feldmann, A. F. Frangi, P. M. Full, B. van Ginneken, A. Hanbury, K. Honauer, M. Kozubek, B. A. Landman, K. März, O. Maier, K. Maier-Hein, B. H. Menze, H. Müller, P. F. Neher, W. Niessen, N. Rajpoot, G. C. Sharp, K. Sirinukunwattana, S. Speidel, C. Stock, D. Stoyanov, A. A. Taha, F. van der Sommen, C.-W. Wang, M.-A. Weber, G. Zheng, P. Jannin, A. Kopp-Schneider, Why rankings of biomedical image analysis competitions should be interpreted with care, *Nature Communications* 9 (1) (2018) 5217, publisher: Nature Publishing Group. doi:10.1038/s41467-018-07619-7.
URL <https://www.nature.com/articles/s41467-018-07619-7>
- [32] A. Arnab, M. Dehghani, G. Heigold, C. Sun, M. Lučić, C. Schmid, ViViT: A Video Vision Transformer, in: *Proceedings of the IEEE/CVF international conference on computer vision*, 2021, pp. 6836–6846.
URL https://openaccess.thecvf.com/content/ICCV2021/html/Arnab_ViViT_A_Video_Vision_Transformer_ICCV_2021_paper.html?ref=https://githubhelp.com

- [33] A. Dosovitskiy, L. Beyer, A. Kolesnikov, D. Weissenborn, X. Zhai, T. Unterthiner, M. Dehghani, M. Minderer, G. Heigold, S. Gelly, J. Uszkoreit, N. Houlsby, An Image is Worth 16x16 Words: Transformers for Image Recognition at Scale, arXiv:2010.11929 [cs] (Jun. 2021). doi:10.48550/arXiv.2010.11929.
URL <http://arxiv.org/abs/2010.11929>
- [34] D. J. Beutel, T. Topal, A. Mathur, X. Qiu, J. Fernandez-Marques, Y. Gao, L. Sani, K. H. Li, T. Parcollet, P. P. B. d. Gusmão, N. D. Lane, Flower: A Friendly Federated Learning Research Framework, arXiv:2007.14390 [cs] (Mar. 2022). doi:10.48550/arXiv.2007.14390.
URL <http://arxiv.org/abs/2007.14390>
- [35] D. Batić, F. Holm, E. Özsoy, T. Czempiel, N. Navab, EndoViT: pretraining vision transformers on a large collection of endoscopic images, *International Journal of Computer Assisted Radiology and Surgery* 19 (6) (2024) 1085–1091. doi:10.1007/s11548-024-03091-5.
URL <https://doi.org/10.1007/s11548-024-03091-5>
- [36] S. Yang, F. Zhou, L. Mayer, F. Huang, Y. Chen, Y. Wang, S. He, Y. Nie, X. Wang, Ö. Sümer, Y. Jin, H. Sun, S. Xu, A. Q. Liu, Z. Li, J. Qin, J. Y. Teoh, L. Maier-Hein, H. Chen, Large-scale Self-supervised Video Foundation Model for Intelligent Surgery, arXiv:2506.02692 [cs] (Jun. 2025). doi:10.48550/arXiv.2506.02692.
URL <http://arxiv.org/abs/2506.02692>
- [37] S. Schmidgall, J. W. Kim, J. Jopling, A. Krieger, General surgery vision transformer: A video pre-trained foundation model for general surgery, arXiv:2403.05949 [cs] (Apr. 2024). doi:10.48550/arXiv.2403.05949.
URL <http://arxiv.org/abs/2403.05949>
- [38] D. Caldarola, B. Caputo, M. Ciccone, Improving Generalization in Federated Learning by Seeking Flat Minima, in: S. Avidan, G. Brostow, M. Cissé, G. M. Farinella, T. Hassner (Eds.), *Computer Vision – ECCV 2022*, Springer Nature Switzerland, Cham, 2022, pp. 654–672. doi:10.1007/978-3-031-20050-2_38.
- [39] P. Foret, A. Kleiner, H. Mobahi, B. Neyshabur, Sharpness-Aware Minimization for Efficiently Improving Generalization, arXiv:2010.01412 [cs] (Apr. 2021). doi:10.48550/arXiv.2010.01412.
URL <http://arxiv.org/abs/2010.01412>
- [40] S. Reddi, Z. Charles, M. Zaheer, Z. Garrett, K. Rush, J. Konečný, S. Kumar, H. B. McMahan, Adaptive federated optimization, version: 5. arXiv:2003.00295 [cs], doi:10.48550/arXiv.2003.00295.
URL <http://arxiv.org/abs/2003.00295>
- [41] K. He, X. Zhang, S. Ren, J. Sun, Deep Residual Learning for Image Recognition, arXiv:1512.03385 [cs] (Dec. 2015). doi:10.48550/arXiv.1512.03385.
URL <http://arxiv.org/abs/1512.03385>
- [42] J. Bromley, I. Guyon, Y. LeCun, E. Säckinger, R. Shah, Signature Verification using a "Siamese" Time Delay Neural Network, in: *Advances in Neural Information Processing Systems*, Vol. 6, Morgan-Kaufmann, 1993.

URL <https://proceedings.neurips.cc/paper/1993/hash/288cc0ff022877bd3df94bc9360b9c5d-Abstract.html>

- [43] P. Luo, R. Zhang, J. Ren, Z. Peng, J. Li, Switchable Normalization for Learning-to-Normalize Deep Representation, *IEEE Transactions on Pattern Analysis and Machine Intelligence* 43 (2) (2021) 712–728. doi:10.1109/TPAMI.2019.2932062.
URL <https://ieeexplore.ieee.org/abstract/document/8781758>
- [44] Z. Liu, H. Mao, C.-Y. Wu, C. Feichtenhofer, T. Darrell, S. Xie, A convnet for the 2020s, in: *Proceedings of the IEEE/CVF conference on computer vision and pattern recognition, 2022*, pp. 11976–11986.
- [45] O. Russakovsky, J. Deng, H. Su, J. Krause, S. Satheesh, S. Ma, Z. Huang, A. Karpathy, A. Khosla, M. Bernstein, et al., Imagenet large scale visual recognition challenge, *International Journal of Computer Vision* 115 (2015) 211–252.
- [46] S. Hochreiter, J. Schmidhuber, Long short-term memory, *Neural Computation* 9 (8) (1997) 1735–1780.
- [47] S. Warnat-Herresthal, H. Schultze, K. L. Shastry, S. Manamohan, S. Mukherjee, V. Garg, R. Sarveswara, K. Händler, P. Pickkers, N. A. Aziz, et al., Swarm learning for decentralized and confidential clinical machine learning, *Nature* 594 (2021) 265–270.
- [48] Hewlett Packard Enterprise, Swarm learning, <https://github.com/HewlettPackard/swarm-learning> (2021).
- [49] E. J. Hu, Y. Shen, P. Wallis, Z. Allen-Zhu, Y. Li, S. Wang, L. Wang, W. Chen, LoRA: Low-rank adaptation of large language models, in: *International Conference on Learning Representations, 2022*.